

2006

# Microstructural evolution during flash annealing of hot rolled 6061 aluminum alloys

Neil Hurley  
*Lehigh University*

Follow this and additional works at: <http://preserve.lehigh.edu/etd>

---

## Recommended Citation

Hurley, Neil, "Microstructural evolution during flash annealing of hot rolled 6061 aluminum alloys" (2006). *Theses and Dissertations*. Paper 915.

This Thesis is brought to you for free and open access by Lehigh Preserve. It has been accepted for inclusion in Theses and Dissertations by an authorized administrator of Lehigh Preserve. For more information, please contact [preserve@lehigh.edu](mailto:preserve@lehigh.edu).

Hurley, Neil D.

Microstructural  
Evolution During  
Flash Annealing  
of Hot Rolled  
6061 Aluminum  
Alloys

January 2006

# **Microstructural Evolution During Flash Annealing of Hot Rolled 6061 Aluminum Alloys**

by

Neil D. Hurley

A thesis

Presented to the Graduate and Research Committee

of Lehigh University

in Candidacy for the Degree of

Master of Science

in

Materials Science and Engineering

December 9, 2005

## Certificate of Approval

This thesis is accepted and approved in partial fulfillment of the requirements for the Master of Science

12/8/2005

Date

---

Wojciech Z. Misiolek  
Thesis Advisor

Slade Cargill  
Chairperson

## Acknowledgements

I would like to thank the institutions and individuals that helped make this research possible. First, I would like to thank DOE contract #DE – FC07 – OIID14191, Alcoa Incorporated, and the ET Foundation for giving me the financial support to go forward with this research. Without their generosity this project would have never been completed.

My gratitude also goes out to my advisor Dr. Wojciech Misiolek whose guidance throughout this project was invaluable. Also, a special thanks goes to Dr. William VanGeertruyden who helped spark my interest in aluminum processing as an undergraduate, and gave me direction on this research whenever it was needed. To my fellow Institute of Metal Forming members and friends Alex Bandar, Heather Browne, Steven Claves, Frank Gift, Mario Epler, Andy Prescott, and Dan Raiser, thank you for making it so easy to come in to the lab everyday.

Without the help of the outstanding research engineering staff of Arlan Bencoter, Dave Ackland, and Bill Mushock, this work would have been far more difficult to complete. I would like to thank them for helping me with all of the metallography and characterization work that this project required.

Finally, I would like to thank all of my friends and family for their love and support over the last few years. To my parents David and Janet, words cannot express the level of gratitude that I have for all that you have done for me

throughout my life, and my girlfriend Maggie Hagerman, thank you for always being there for me whenever I needed anything.

# Table of Contents

Certificate of Approval.....	ii
Acknowledgements.....	iii-iv
List of Tables.....	vii
List of Figures.....	viii-xi
Abstract.....	1-2

## 1.0 Introduction

1.1 Aluminum Rolling Background.....	3
1.1.1 Material – AA6xxx.....	3-4
1.1.1.1 Metallurgy of AA6xxx.....	4-6
1.1.1.2 Common Applications.....	6-7
1.1.2 Hot Rolling.....	7
1.1.2.1 Common Industrial Rolling Procedure for AA6xxx Sheet.....	7-9
1.1.2.2 State of Stress and Strain Present During Rolling Deformation.....	9-12
1.1.2.3 Deformation Zone Geometry.....	12-13
1.1.2.4 Differences Between Hot and Cold Rolling.....	14-15
1.1.3 Recrystallization.....	15
1.1.3.1 Static and Dynamic Recrystallization.....	16
1.1.3.2 Continuous and Dynamic Recrystallization.....	17-18
1.1.3.3 Effects of Processing Parameters on Stored Energy.....	18-21
1.1.3.4 Effects of Alloying Additions on Slowing Recrystallization Kinetics.....	21
1.1.3.5 Johnson – Mehl – Avrami – Kolmogorov Recrystallization Kinetics.....	22-23
1.1.4 Microstructural Evolution.....	24
1.1.4.1 Effects of Grain Size and Deformation Texture on Microstructural Evolution During Annealing.....	24-26
1.2 Microstructural Characterization: Electron Backscatter Diffraction.....	26-30

## 2.0 Procedure

2.1 Material.....	31
2.2 Lab Scale Hot Rolling and Flash Annealing Experiments.....	32
2.2.1 Lab Scale Hot Rolling Equipment Set – Up.....	32-34
2.2.2 Rolling Schedules.....	34-36
2.2.3 Flash Annealing.....	36-37
2.3 Light Optical Microscopy.....	37
2.3.1 Sample Preparation.....	37-38
2.3.2 Microstructural Characterization.....	38-39

2.4 Electron Backscatter Diffraction.....	39
2.4.1 Sample Preparation.....	39
2.4.2 Microstructural Characterization.....	39-42
<b>3.0 Results</b>	
3.1 Light Optical Microscopy.....	43
3.1.1 Deformed and Annealed Microstructures.....	43-51
3.1.2 Recrystallization Kinetics.....	52-55
3.2 Electron Backscatter Diffraction.....	56
3.2.1 Microstructural Characterization.....	56-60
3.2.2 Non-Uniform Recrystallization Kinetics.....	61-64
<b>4.0 Discussion and Future Work</b>	
4.1 Effects of Processing Parameters and Alloying on Recrystallization Kinetics.....	65-68
4.2 Non-Uniform Recrystallization Kinetics.....	69-71
4.3 Quantitative Analysis of Recrystallization Kinetics.....	72-63
4.4 Future Work.....	73-74
<b>5.0 Conclusions.....</b>	<b>75-76</b>
<b>6.0 References.....</b>	<b>77-79</b>
<b>Vita.....</b>	<b>80</b>



## List of Tables

<b>Table I:</b> Alloy composition ranges for specific 6xxx series aluminum alloys.....	4
<b>Table II:</b> Effect of Tempering on Material Properties for AA6061.....	6
<b>Table III:</b> Summary of Lab Scale Hot Rolling Conditions and the sample designation.....	34
<b>Table IV:</b> Multi-Pass Rolling Schedule for a 75% Total Reduction.....	36
<b>Table V:</b> Multi-Pass Rolling Schedule for a 90% Total Reduction.....	36
<b>Table VI:</b> Processing Conditions for EBSD Analysis Samples.....	40
<b>Table VII:</b> Chart showing the percent of recrystallized grains present after various flash annealing times for various processing conditions.....	52
<b>Table VIII:</b> Volume Fraction of percent recrystallization at the center and surface for four processing conditions exhibiting differences in kinetics at the surface versus the center of the strip thickness.....	61

## List of Figures

<b>Figure 1.</b> Common thermomechanical processing stages for AA6xxx sheet.....	9
<b>Figure 2.</b> Shear deformation and heavy deformation during hot rolling.....	10
<b>Figure 3.</b> Force distribution applied to the work piece during hot rolling.....	11
<b>Figure 4.</b> Comparison of homogeneous and redundant deformation.....	13
<b>Figure 5.</b> Schematic diagram showing the progression of how serrated grains will transform to new equiaxed grains after further deformation.....	18
<b>Figure 6.</b> The effect of strain on recrystallization kinetics.....	19
<b>Figure 7.</b> The JMAK kinetics for recrystallization for various annealing times.....	23
<b>Figure 8.</b> Volume fraction of cube, Brass, Copper and S texture components versus percent recrystallized for hot rolled FCC metal.....	26
<b>Figure 9.</b> Set up for an electron back scatter diffraction pattern, and the collected Kikuchi pattern.....	27
<b>Figure 10.</b> An example an EBSD pattern with the indexed crystallographic planes identified.....	29
<b>Figure 11.</b> Misorientation histogram for a material that has a high volume fraction of recrystallized grains.....	30
<b>Figure 12.</b> Diagram representing the area that the rolling samples were sectioned from the DC cast billet.....	32
<b>Figure 13.</b> The sample orientation for LOM and EBSD analysis. The colored surface represents the area that was used for analysis.....	38
<b>Figure 14.</b> The relative position of the two EBSD area scans taken for each sample.....	41
<b>Figure 15.</b> Processing Conditions Set A: High Cr content, rolling temperature of 482°C, Single Pass, 90% total reduction. A) As Deformed, B) 3 second anneal, C) 5 second anneal, D) 7 second anneal, E) 10 second anneal.....	44

**Figure 16.** Processing Conditions Set B: High Cr content, rolling temperature of 482°C, 3 Pass, 90% total reduction. A) As Deformed, B) 3 second anneal, C) 5 second anneal, D) 7 second anneal, E) 10 second anneal.....45

**Figure 17.** Processing Conditions Set C: Low Cr content, rolling temperature of 482°C, 3 Pass, 90% total reduction. A) As Deformed, B) 3 second anneal, C) 5 second anneal, D) 7 second anneal, E) 10 second anneal.....46

**Figure 18.** Processing Conditions Set F: Low Cr content, rolling temperature of 482°C, 1 Pass, 75% total reduction. A) As Deformed, B) 3 second anneal, C) 5 second anneal, D) 7 second anneal, E) 10 second anneal.....47

**Figure 19.** Processing Conditions Set H: High Cr content, rolling temperature of 400°C, 1 Pass, 75% total reduction. A) As Deformed, B) 3 second anneal, C) 5 second anneal, D) 7 second anneal, E) 10 second anneal.....48

**Figure 20.** Processing Conditions Set I: Low Cr content, rolling temperature of 400°C, 1 Pass, 75% total reduction. A) As Deformed, B) 3 second anneal, C) 5 second anneal, D) 7 second anneal, E) 10 second anneal.....49

**Figure 21.** Processing Conditions Set L: High Cr content, rolling temperature of 400°C, 1 Pass, 90% total reduction. A) As Deformed, B) 3 second anneal, C) 5 second anneal, D) 7 second anneal, E) 10 second anneal.....50

**Figure 22.** Processing Conditions Set M: Low Cr content, rolling temperature of 400°C, 1 Pass, 90% total reduction. A) As Deformed, B) 3 second anneal, C) 5 second anneal, D) 7 second anneal, E) 10 second anneal.....51

**Figure 23.** Percent of recrystallized grains versus time with high and low Cr levels for a single pass reduction of 75% at 400°C (750°F).....53

**Figure 24.** Percent of recrystallized grains versus time with high and low Cr levels for a single pass reduction of 90% at 400°C (750°F).....53

**Figure 25.** Percent of recrystallized grains versus time with 75% and 90% reductions for a high Cr alloy hot rolled with one pass at 400°C (750°F).....54

**Figure 26:** Percent of recrystallized grains versus time with 75% and 90% reductions for a low Cr alloy hot rolled with one pass at 400°C (750°F).....54

**Figure 27:** Percent of recrystallized of grains versus time for deformation temperatures of 400°C (750°F) and 482°C (900°F) reductions for a low Cr alloy hot rolled with one pass to a 75% reduction.....55

**Figure 287:** Percent of recrystallized grains versus time for single pass versus multi pass deformation to a total reduction of 90% at 482°C (900°F) with a high Cr content.....55

**Figure 29.** EBSD area scan for a sample with low Cr content, rolled to a 75% reduction in a single pass at 400°C (750°F) taken at the sample surface after a 5 second anneal. A) EBSD microstructural image, B) EBSD image showing subgrain formation.....57

**Figure 30.** EBSD area scan for a sample with low Cr content, rolled to a 75% reduction in a single pass at 400°C (750°F) taken at the sample center after a 5 second anneal. A) EBSD microstructural image, B) EBSD image showing subgrain formation. The black arrows mark areas of deformed material.....58

**Figure 31.** EBSD area scan for a sample with low Cr content, rolled to a 90% reduction in a single pass at 400°C (750°F) taken at the sample surface after a 3 second anneal. A) EBSD microstructural image, B) EBSD image showing subgrain formation.....59

**Figure 32.** EBSD area scan for a sample with high Cr content, rolled to a 90% reduction in a single pass at 400°C (750°F) taken at the sample surface after a 3 second anneal. A) EBSD microstructural image, B) EBSD image showing subgrain formation. The black areas point to areas of recrystallized material.....60

**Figure 33.** Misorientation histograms for EBSD scans taken at the surface of a sample with high Cr content deformed to a 75% reduction in a single pass at 400°C (750°F) (Condition H). A) 3 second anneal, B) 5 second anneal, C) 7 second anneal.....62

**Figure 34.** Percent of recrystallized grains for processing condition H at the surface and center.....63

**Figure 35.** Percent of recrystallized for processing condition I at the surface and center.....63

**Figure 36.** Percent of recrystallized grains for processing condition L at the surface and center.....64

**Figure 37.** Percent of recrystallized for processing condition M at the surface and center.....64

## **Abstract**

During hot deformation of Al-Mg-Si alloys, a non-uniform microstructure is developed due to differences in localized strain. Specifically, during bulk deformation processes such as hot rolling, localized strain cause a deleterious surface microstructure evolution creating surface imperfections such as ridging or roping which lead to scrapping of the material. Physical simulations were performed to examine the effects of processing parameters such as deformation temperature, total reduction, rolling schedule and Cr content on the overall microstructural evolution, specifically the volume percent of recrystallized grains present in the material at various flash annealing times, through the thickness of the deformed sheet. The non-isothermal flash annealing is used to simulate the microstructural evolution that is occurring immediately after the sheet is leaving the rolls after deformation. Overall, the kinetics of recrystallization for the samples when considering processing parameters and Cr content followed the trends predicted by JMAK curve kinetics.

The deformed and annealed material were characterized using Light Optical Microscopy (LOM) and Electron Backscatter Diffraction (EBSD). These two techniques allowed for a quantitative analysis of the volume fraction of recrystallized material present versus flash annealing time. Specifically, EBSD was used to quantify the difference in recrystallization kinetics at the sample surface and mid-thickness. The results showed that the surface showed elevated

kinetics when compared to the sample mid-thickness which follows the expected trends when considering the state of shear stress created at the surface of hot rolled aluminum sheet due to friction between the rolls and the work piece. The goal is to use the information created from this experiment as input data into numerical models currently being developed for microstructure prediction.

# 1.0 Introduction

## 1.1 Aluminum Rolling Background

### 1.1.1 Material – AA6xxx

Aluminum is important to the metals processing industry because of its combination of light weight, high strength, corrosion resistance and flexibility of processing techniques. These material characteristics allow for aluminum to replace more traditional materials such as steel and cast iron without sacrificing performance or reliability. Aluminum production begins with the mining of bauxite from areas of the world such as Australia and Guyana. After the bauxite has been mined, the aluminum is extracted from the ore by a process of electrolytic reduction. The process of extracting aluminum from bauxite ore is energy intensive which is one of the driving forces to develop processing techniques that will minimize aluminum scrap. Once the aluminum has been separated out from the ore, it can then be combined with other elements to create the desired properties associated with various different aluminum alloys. The most common alloying elements for aluminum are copper, magnesium, silicon, and zinc. Another important characteristic of aluminum alloys is that some are heat-treatable which allow for an improvement in strength after an optimized heat treatment. This is an important property of specific aluminum alloys because it allows for the mechanical properties of the material to be tailored to the end application. For aluminum alloys that do not increase their strength from heat treatment, the most



common technique for strength improvement is work hardening and solid solution strengthening. Aluminum also exhibits strong corrosion resistance because of the thin oxide film ( $Al_2O_3$ ) that forms on the surface. Aluminum alloys can be processed with a variety of techniques to fit specific applications. These processes include methods several casting methods or deformation processing techniques such as rolling, extrusion, forging, or drawing. This flexibility in processing makes it possible for aluminum to be manufactured to satisfy almost any geometric or performance requirement.

#### 1.1.1.1 Metallurgy of AA6xxx

In this research AA6061 was chosen due to its good weldability, corrosion resistance, immunity to stress corrosion cracking, and good formability [1]. AA6xxx alloys are also heat treatable which allows for an increase in strength after an optimized heat treatment schedule. The major alloying elements in AA6061 are silicon and magnesium. The chemistry range for this alloy can be seen in Table I.

**Table I:** Alloy composition ranges for AA6061 aluminum alloys.<sup>2</sup>

Alloy Designation	Si	Fe	Cu	Mn	Mg	Zn	Cr	Ti
AA6061	0.4-0.8	0.7	0.15-0.40	0.15	0.08-0.12	0.25	0.04-0.35	0.15

The alloying elements of magnesium and silicon combine to form a precipitation phase  $Mg_2Si$ , which is the major component responsible for

increasing the strength of 6xxx aluminum alloys. The precipitation of this secondary phase out of solid solution has been examined in great detail to maximize its effectiveness on age-hardening [3]. The initial stage of the formation of  $Mg_2Si$  particles begins in the solid solution and occurs during ageing when the two elements cluster together to form Guinier-Preston (GP) zones. Following this clustering,  $\beta''$   $Mg_2Si$  forms as coherent Widmanstätten needles that lie in the [100] crystallographic direction. Next, the  $\beta''$  needles transform in semi-coherent  $\beta'$  rods. These rods are associated with the maximum ageing strength because they are semi-coherent and therefore the most effective at retarding dislocation movement. Finally, the  $\beta'$  rods are transformed into  $\beta$   $Mg_2Si$  platelets. Along with forming precipitates, magnesium and silicon also serve the function of solid solution strengtheners [3].

Other alloying elements present in AA6061 such as copper, zirconium, and chromium also serve a purpose to alter the microstructure. Copper is added for its ability to increase solid solution strengthening, and zirconium and chromium act to increase the recrystallization temperature and inhibit recovery and recrystallization [4]. A more in depth discussion concerning the effects of chromium on the kinetics of recrystallization is presented in section 1.1.3.2.

Because AA6xxx series aluminum alloys are heat treatable, there can be large variations in mechanical strength associated with different heat treatment schedules. These heat treatments are important to understand prior to metal

forming because the manufacturer will tailor their processing and heat treatment schedule based on the properties of the wrought product. Also, the heat treatment schedule is critical in creating a uniform distribution and desirable particle size of the Mg<sub>2</sub>Si phase. These alloys are typically delivered in the T6 condition. This signifies a solution treatment, quenching, and artificial ageing to create a high strength alloy. Table II shows the difference in various material properties between the T6 temper and an annealed product, designate O, with no artificial ageing or solution heat treatment for AA6061. Note the substantial increase in yield strength, and ultimate tensile strength for the tempered alloy as a result of the optimized precipitation of the Mg<sub>2</sub>Si second phase particles.

**Table II:** Effect of Tempering on Material Properties for AA6061.<sup>2</sup>

Temper	UTS (ksi)	YS (ksi)	Elongation (%)	Brinell Hardness
AA6061 - T6	45	40	12	95
AA6061 - O	18	8	25	30

### 1.1.1.2 Common Applications

The majority of 6xxx aluminum alloys are used as medium strength structural components. This material is most commonly extruded and is desirable due to its formability, corrosion resistance, high strength, and resistance to stress corrosion cracking. Although AA6xxx is most commonly used for extrusion, this alloy series is gaining popularity in sheet forming because of the aforementioned properties. Specifically, these alloys are becoming more popular in the next

generation of automobile body panel sheet. The potential weight savings associated with using aluminum body sheet, instead of the more traditional steel, can greatly decrease the weight of an automobile. Compared to more common alloys used for aluminum sheet forming such as 2xxx and 5xxx series alloys, 6xxx series alloys stand out because of their combination of mechanical properties and their ability to strengthen significantly during the paint bake cycles at sufficient temperatures [5]. This high strength makes the application of this alloy well suited for automotive body panels because of its ability to be dent resistant while remaining light weight.

## **1.1.2 Hot Rolling**

### **1.1.2.1 Common Industrial Rolling Procedure for AA6xxx Sheet**

In commercial production of AA6xxx sheet, the material goes through a specific series of deformation and heat treatment steps that can be generalized by the term thermomechanical processing. Controlling the end properties of a rolled sheet is highly dependant on this thermomechanical treatment. Figure 1 shows a schematic representation of the common processing procedure for AA6xxx sheet. The first step in forming a hot rolled sheet is to direct chill (DC) cast the ingots. Common dimensions for these ingots are 600 mm thick, 2 m wide and between 4 – 9 m long [5]. Often during the DC casting processing surface defects are created and therefore must be removed before the rolling process can begin. Prior to deformation, the ingots are heated to between 480°C (900°F) and 580°C (1075°F)

for up to 48 hours depending on the exact size of the ingot. This is an important stage of the sheet forming process because it creates a homogenous material and eliminates any chemical segregation that may have occurred during the DC casting process. Next, the heated ingots are deformed with a reverse break down mill followed by a high speed multi stand tandem mill. Typically the breakdown mills will reduce the thickness of the sheet to 25 – 40 mm and the multi-stand hot rolling process will reduce the sheet to a final thickness between 3 – 6 mm [5]. After these hot rolling steps, the sheet is cooled and cold rolled to final dimensions between 0.8 – 1.2 mm.

The sheet is then annealed to obtain maximum age hardening and formability. This heat treatment dissolves any hardening phases and quenches in any alloying elements in to solid solution. By eliminating any hardening phases this will increase the formability of the rolled AA6xxx sheet which is important because the final rolled sheet is often stamped to reach a desired geometry for various end applications. Finally, for body panel applications, the sheet is painted and then baked to create the final piece. It is during this paint bake cycle that the 6xxx aluminum alloy increases its strength by precipitating the  $Mg_2Si$  phase to aid in the increase in mechanical properties.

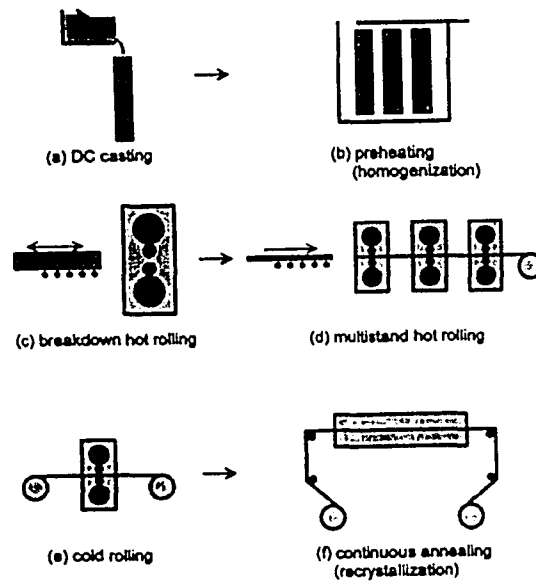


**Figure 1.** Common thermomechanical processing stages for AA6xxx sheet.<sup>5</sup>

### 1.1.2.2 State of Stress and Strain Present During Rolling Deformation

Rolling is a processing technique that commonly creates thin sheets or strips by passing material through a series of rolling deformation steps, with reducing roll gap size, to obtain the desired thickness. It has been found that there is a gradient in the state of stress experienced by the work piece during rolling [6]. Generally, shear stress is present at the surface, while plane strain compression exists in the center (Figure 2).

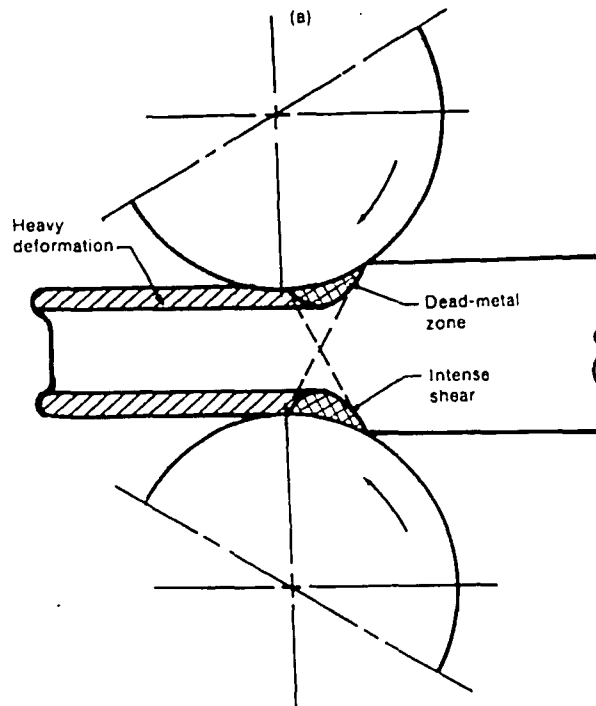


**Figure 2.** Shear deformation and heavy deformation during hot rolling<sup>6</sup>

Figure 3 shows a schematic of the forces acting on the work piece during rolling deformation. It is also important to note that the velocity of the material entering the rolls is traveling slower than the material exiting the rolls ( $V_f > V_o$ ) [7]. Between the entry plane and the neutral point, labeled N in Figure 3, the sheet is moving slower than the roll surface so the friction acts to draw in the material. The opposite holds true on the exit side of the roll, where the material speed is faster than the roll speed and the friction acts to slow the material passing through the rolls.

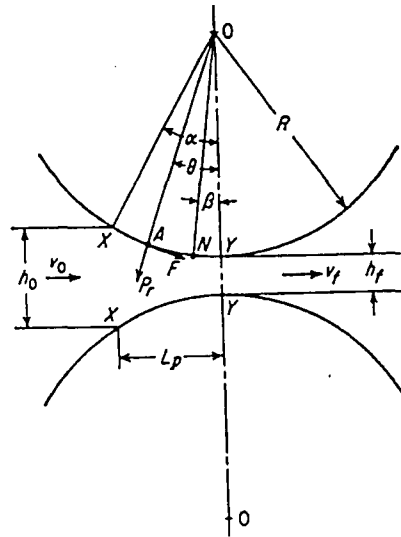


**Figure 3.** Force distribution applied to the work piece during hot rolling.<sup>7</sup>

A strain gradient is created through the thickness of the work piece during deformation that creates a non-uniform distribution of stored energy. Because for certain geometries there is little change in width of the work piece during sheet rolling, this is considered to be plane strain deformation [7]. Friction between the rolls and work piece also plays an important roll in determining the states of stress and strain present at the surface and center of the work piece during deformation. This frictional force that exists between the rolls and the work piece creates a state of shear stress at the surface of the deformed sample. This shear stress is created by a difference in velocity at different points through the thickness of the work piece traveling through the rolls. The surface of the rolled sample will experience a lower average velocity through the rolls because of the sticking friction versus the center of the sample which will not be experiencing the sticking friction and



will therefore travel through at a faster average velocity. An average velocity is used because the velocity of the material entering the rolls is different than the velocity of the material exiting the rolls after deformation.

### **1.1.2.3 Deformation Zone Geometry**

The creation of strain gradients during deformation can also be attributed to the concept of redundant work. Redundant work is due to internal distortion in excess of that needed to produce the desired shape [8]. If the deformation were ideal, planar sections would remain unchanged as the deformation process occurs. This is not the case in hot rolling, where there is the presence of internal shearing that causes a distortion of the plane sections as they pass through the deformation zone. The level of internal shearing can be related to the friction between the work piece and the rolls and the redundant work. A schematic comparing homogeneous deformation to redundant deformation can be seen in Figure 4. This redundant work will cause the end material to be more deformed and therefore harder and less ductile than if the deformation were homogeneous.

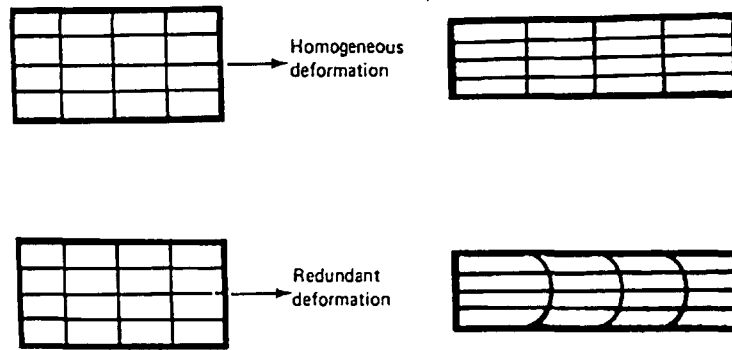


**Figure 4.** Comparison of homogeneous and redundant deformation.<sup>8</sup>

The shape of the deformation zone will have a large effect on the amount of redundant work and the contribution of frictional work during rolling. This deformation zone will also have a strong influence on the stored energy created during deformation [8]. Deformation zone geometry can be described by the parameter  $\Delta$  which is defined as the ratio of the mean thickness of the rolled sheet to the contact arc of the roll. For rolling, this parameter is defined in equation 1.1. In this formula,  $\Delta$  increases with ratio of the sheet thickness to the roll radius. As the  $\Delta$  value increases, the amount of inhomogeneous flow increases, which increases the strain gradient from the surface to the center of the rolled piece [8].

$$\Delta = \frac{(2 - r)}{2} \sqrt{\frac{h_o}{rR}} \quad (1.1)$$

Where:

$\Delta$  = Deformation Zone Geometry

$r$  = Reduction

$h_0$  = Initial sheet thickness

$R$  = Roll radius

#### 1.1.2.4 Differences Between Hot and Cold Rolling

For the entire rolling process, the stage associated with highest levels of overall reduction is hot rolling. The difference between hot rolling and cold rolling is that hot rolling is conducted at temperatures greater than 0.5 times the melting temperature ( $T > 0.5T_m$ ). This difference between hot and cold rolling creates significant differences in the amount of overall deformation a piece will be able to experience, the surface finish, and the flow stress.

During hot rolling, the majority of the overall reduction is completed to get the sheet thickness close to its desired gauge. Hot rolling allows for larger amounts of reduction because the work is done at elevated temperatures which lowers the flow stress during deformation, and therefore lowers the level of stored energy when compared to a sample cold rolled under similar conditions. The effect of stored energy created during hot rolling can be seen in later processes of recovery and recrystallization that will be discussed in greater depth in section 1.1.3.1. During hot rolling it is more difficult to account for inhomogeneous deformation and friction conditions [7]. Therefore, in hot rolling the flow stress is a function of the rolling temperature and the strain rate which is governed by the speed of the rolls and reduction per pass [9].

Cold rolling is most often used as the final step in the rolling process. It is performed around room temperature, and its purpose is to create a good surface finish free of imperfections. The study of flow stress, when considering cold rolling, is better understood than that of hot rolling. The values for flow stress are

not as highly dependant upon strain rate [7]. For cold rolling, the level of deformation created during processing is higher than that of a sample processed similarly under hot rolling conditions. There will be a higher level of work hardening and sharper strain gradients associated with cold rolling. This is why there are annealing treatments applied to the work piece after cold rolling that relieve some of the strain hardening and stored energy created during cold rolling which may limit formability.

### **1.1.3 Recrystallization**

Recrystallization is an important phenomenon that occurs during hot deformation or upon annealing. For aluminum, it is important to understand the rate of recrystallization when considering processing parameters because overall strength and surface quality need to be tailored to meet end requirements. Careful consideration must be given to the definition of recrystallization because it closely resembles other processes that relieve internal stresses created during deformation such as recovery. Recrystallization is defined as the formation of a new grain structure in a deformed material by the formation and migration of high angle boundaries (misorientations between  $10^\circ - 15^\circ$ ) driven by stored energy created during deformation [10]. From this definition of recrystallization, it can be seen that the rate of recrystallization is a function of the stored energy that is created during deformation by varying processing parameters and heat treatments.

### 1.1.3.1 Static and Dynamic Recrystallization

Static recrystallization occurs when a hot deformed material is annealed after processing. During this process the material will nucleate and grow recrystallized grains at a rate specific to the prior mechanical processing schedule. It has been shown in the literature that the recrystallization behavior will be strongly dependant on the Zener – Hollomon parameter which is a variable that incorporates strain rate and deformation temperature [11]. The kinetics for static recrystallization can be modeled using the Johnson – Mehl –Avrami – Kolmogorov (JMAK) equation which will be explained in more detail in section 1.1.3.5. For traditional static recrystallization experiments conducted on the material used in this experiment, the traditional annealing times are between two and three hours.

Dynamic recrystallization is a process by which recrystallized grains nucleate and grow during hot deformation instead of during a post processing heat treatment. This process of dynamic recrystallization is predominant in materials with low stacking fault energies such as Cu, Ni, and  $\gamma$ -Fe that have slow recovery processes. For a material like Al that has a high stacking fault energy, the material will tend to dynamically recover instead of dynamically recrystallizing to reduce the level of stored energy created during hot rolling.

### 1.1.3.2 Continuous and Geometric Dynamic Recrystallization

Continuous Dynamic Recrystallization (cDRX) is a process that differs from traditional Dynamic Recrystallization theory. For the case of cDRX, subgrain structures will evolve into high angle misorientation grains during deformation. After deformation to large strains at elevated temperatures, a microstructure consisting of predominantly high angle boundaries may be formed. This microstructure may appear to be similar to conventional dynamically recrystallized grains, but for cDRX there is no recognizable nucleation or growth of recrystallized grains.

A similar type of recrystallization that occurs during deformation is known as Geometric Dynamic Recrystallization (gDRX). This phenomenon is a subset of cDRX in that it is not a traditional nucleation and growth process. Instead, as the grains are deformed under high strains, they create a fine equiaxed structure with an average grain size approximately on the order of subgrain size [12]. The process of developing gDRX grains begins when the grains begin to flatten and exhibit serrated boundary characteristics. As these serrations grow larger they begin to impinge on each other and start to form new equiaxed grains when the high angle boundaries join. A schematic representing the growth of serrated grain boundaries into equiaxed grains can be seen in Figure 5.

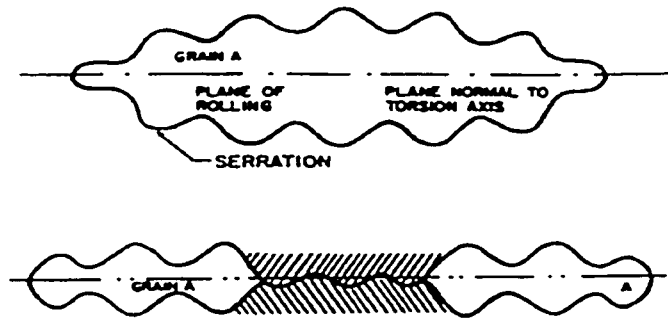


**Figure 5.** Schematic diagram showing the progression of how serrated grains will transform to new equiaxed grains after further deformation.<sup>13</sup>

### 1.1.3.3 Effects of Processing Parameters on Stored Energy

The three most important processing parameters that affect stored energy levels within a work piece deformed by rolling are strain, strain rate, and deformation temperature. These processing parameters will ultimately dictate the final rate of recrystallization a sample will experience upon heat treatment.

Strain is a measure of a materials response to an applied stress through a change in shape and/or size. For the case of forming processes, such as rolling, strain is used to gauge the level of deformation a work piece experiences during processing. Another important factor related to overall stored energy is the strain rate. Strain rate, in rolling, is governed by the speed of the rolls and the amount of reduction for a given pass. The level of strain and strain rate that a sample experiences dictates the stored energy within a deformed sample and therefore the kinetics of recrystallization a sample will undergo during annealing. As the overall strain and strain rate increases, assuming all other processing conditions to

be equal, the kinetics of recrystallization increases. A general example of the effects of increasing strain on recrystallization kinetics for aluminum can be seen in Figure 6. From this figure, a significant decrease in recrystallization time can be seen with increasing strain.

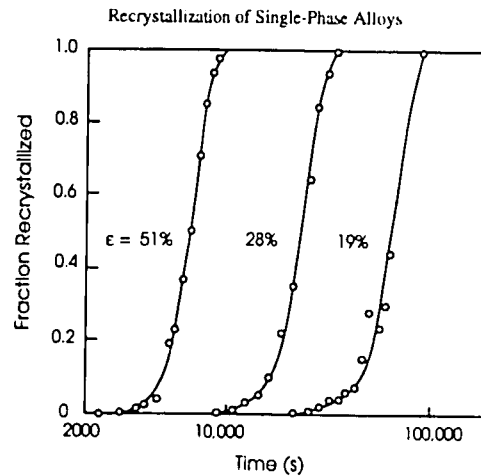


**Figure 6.** The effect of strain on recrystallization kinetics of aluminum annealed at 350°C.<sup>14</sup>

The temperature of the work piece during deformation also has a large effect on the level of stored energy. Processing at elevated temperatures, for materials such as aluminum, allows for some dynamic recovery to occur. The reason for this phenomenon is linked to aluminum's high stacking fault energy, which makes it easier for dislocation to climb and cross slip which lowers the stored energy created during deformation [15]. Also, processing materials at elevated temperatures lowers the flow stress during deformation. This lower flow stress also contributes to a decrease in stored energy versus a work piece formed at



a lower temperature. By combining the effects of lowered flow stress and potential recovery mechanisms present in aluminum by increasing deformation temperature, a slower rate of recrystallization can be expected because of lower levels of stored energy.

Temperature gradients are also created during processing that affect the microstructural evolution during hot rolling and subsequent annealing. Most often, the temperature of the rolls during deformation are cooler than the work piece. This difference in temperature can cause a flux of heat outward from the work piece to the rolls and the surrounding atmosphere. Especially for aluminum alloys, which have a high thermal conductivity, this heat loss creates a thermal gradient within the work piece during deformation. This thermal gradient can lead to differences in flow stress values between the surface and the center of the material which will create a gradient in stored energy. Other factors also contribute to this thermal gradient. Friction between the rolls and the work piece will aid increasing the temperature at the surface of rolled sheet. Also the non-uniform deformation will create thermal gradients from the surface to the center of the material due to the heat generated during deformation. The contribution of heat from deformation will increase as the total reduction increases. These latter phenomena help to balance the heat lost by contact between the heated sheet and the cooler rolls. Overall, the deformation temperature, and subsequent temperature gradient through the thickness of the sheet during deformation, is a complex

process that requires careful balance to minimize the potential thermal gradients and subsequent stored energy gradients.

#### **1.1.3.4 Effects of Alloying Additions on Slowing Recrystallization Kinetics**

There are ways to slow the kinetics of recrystallization in aluminum alloys through alloying elements. Two of the more common alloying elements to impede recrystallization in aluminum alloys are chromium and manganese. Chromium and manganese are added as a minor impurity with a concentration of between 5 – 50 ppm in AA6xxx series aluminum alloys [4]. When these elements are added, they can have several effects on the material besides slowing down the kinetics of recrystallization. They can influence the electrical resistivity, stress corrosion cracking, and strength. The most important effect of these additions in aluminum is to control the grain structure. Chromium and manganese have low diffusion rates in aluminum and form a fine dispersed phase in wrought aluminum products. This dispersed phase inhibits nucleation and grain growth which aid in controlling the microstructure [4]. This is especially helpful during heat treatment processes where higher temperature facilitates traditional nucleation and growth associated with recrystallization.

### 1.1.3.5 Johnson – Mehl – Avrami - Kolmogorov Recrystallization Kinetics

The resulting kinetics of static recrystallization during heat treatment after deformation can be described by the Johnson - Mehl - Avrami - Kolmogorov (JMAK) equation developed in the 1930's. This equation assumes that nuclei are formed at a rate  $N$  and that grains grow in to the deformed material at a linear rate  $G$  [15]. Initially, as these new grains begin to grow in to the deformed material, they grow very rapidly until there are enough new grains growing at once to impinge on each other and the rate of recrystallization begins to decrease. This growth rate will begin to approach zero as the volume fraction of new recrystallized grains ( $X_v$ ) reaches 1 [14]. This phenomenon is described by the JMAK equation (1.2).

$$X_v = 1 - \exp(-Bt^n) \quad (1.2)$$

Where:

$X_v$  = Volume Fraction of Recrystallized Material

$B$  = constant based on nucleation and growth kinetics

$t$  = time

$n$  = geometry of the activated growth sites

For the JMAK equation it is assumed that the nucleation and growth rate remain constant during recrystallization and the nucleation sites are randomly distributed. The variable  $n$  in equation 1.2 is known as the Avrami exponent and for most three dimensional conditions with a constant nucleation rate this value is

4. This value will decrease if the nucleating grains are constrained by geometry and are only allowed to grow in one or two dimensions [15]. A common JMAK plot is shown in Figure 7. This figure shows that a linear relationship can be drawn between  $\ln(t)$  and  $\{\ln[1 / (1-X_v)]\}$  with the slope of the function producing the Avrami exponent. This model gives a good baseline representation of the kinetics of recrystallization, but a more detailed approach must be taken to make a precise quantitative analysis of the recrystallization process in more complex alloys such as AA6061. One of these models is known as the Microstructural Path Methodology proposed by Vandermeer and Rath [15]. This model takes in to account more realistic grain geometries during recrystallized grain growth and makes alterations to the grain impingement theory.

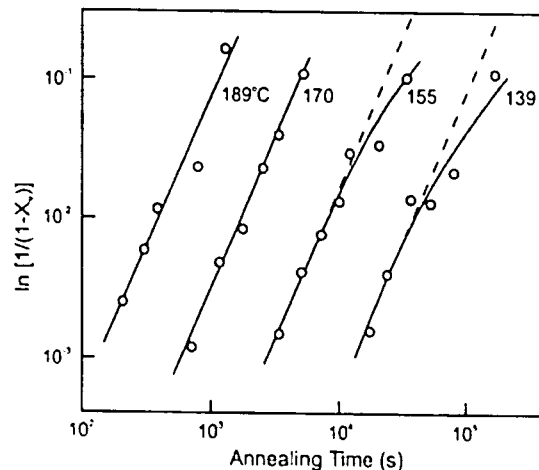


**Figure 7.** The JMAK kinetics for recrystallization for various annealing times for an aluminum alloy containing 0.0068 at % Cu deformed 40% by rolling<sup>15</sup>

## **1.1.4 Microstructural Evolution**

### **1.1.4.1 Effects of Grain Size and Deformation Texture on Microstructural Evolution During Annealing**

Microstructures and textures that develop during deformation directly influence the microstructural changes that occur during recrystallization [13]. It has been found that deforming grains subdivide into misoriented regions and that high angle dislocation boundaries form during deformation. More recent work has examined the effects of grain subdivision, grain size, and crystallographic orientations using Electron Back Scatter Diffraction (EBSD) to quantitatively study the effects of these conditions on the evolution of deformed microstructures [17].

The initial grain size has a strong influence on the microstructural evolution of a deformed sample during heat treatment [15]. Specifically, the rate of recrystallization is greatly affected by the initial grain size present in the material. A material with a finer initial grain size exhibits a greater recrystallization rate upon heating because of the increased availability of nucleation sites. The increased availability of nucleation sites can be attributed to the larger area of grain boundaries present in a fine grained material which are the preferred nucleation sites for recrystallization. Consideration must also be given to any inhomogeneities formed during deformation such as shear bands. These

bands are more readily formed in materials with a coarse grain structure and are considered to be another set of nucleation sites besides grain boundaries [18].

In aluminum alloys it has been shown that the differences in texture formed after hot rolling and annealing lead to differences in recrystallization kinetics when the material is cold rolled and annealed [19]. Variations in texture components are created in a material during deformation which allow for inhomogeneous recrystallization during heat treatment. Properties such as formability and surface finish rely heavily on the crystallographic orientation of the grains present at the surface and throughout the sheet. For example, a weak widely scattered cube recrystallization texture significantly increases the limiting dome height in sheet metal forming [15]. Also, the local distribution, or microtexture, has been identified as the main reason for the presence of the surface defect known as roping or ridging which can be attributed to the presence of bands of similar orientation [20].

The initial deformed state of aluminum after hot rolling is important in explaining the final recrystallized texture. Because recrystallization is dependant upon prior thermomechanical treatments, a correlation between the two stages of processing is important to understand. During hot rolling, the texture of the aluminum sheet is mostly the typical FCC (copper) rolling texture. In this texture, most orientations are assembled along the  $\beta$  fiber, which runs from the Copper (C) orientation  $\{211\}\langle 111\rangle$  through the S orientation  $\{123\}\langle 634\rangle$  to the Brass (B) orientation  $\{110\}\langle 112\rangle$ [21]. These primary texture components in the deformed

state give way to the highly symmetric cube texture component  $\{001\}\langle 100 \rangle$  after recrystallization [22]. Figure 8 shows the volume fraction of cube, B, C, and S components as a function of percent recrystallized for hot rolled FCC material at 90% reduction, showing the increase of the cube texture component and subsequent decrease of B, C, and S components. It has been shown for the material used in this experiment that the overall recrystallization texture is random; instead of predominantly cube [13]

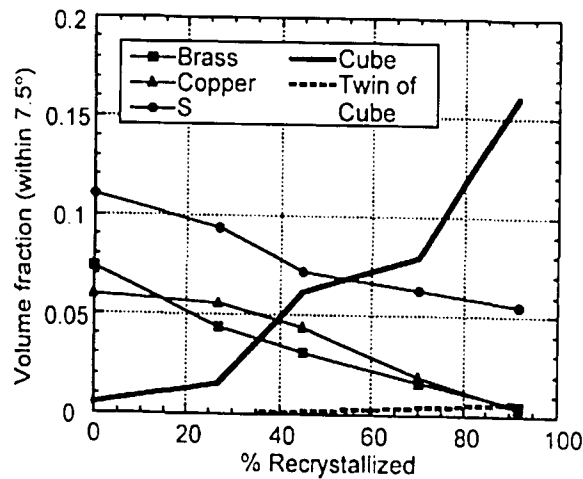


Figure 8. Volume fraction of cube, Brass, Copper and S texture components versus percent recrystallized for hot rolled pure aluminum<sup>22</sup>

## 1.2 Microstructural Characterization: Electron Backscatter Diffraction

Traditional techniques for material characterization, such as Light Optical Microscopy (LOM), have limitations in the information that it can provide about a

material. To obtain more precise information about recrystallization and texture development during deformation processing it is beneficial to use a Scanning Electron Microscope (SEM) integrated with an Electron Backscatter Diffraction Detector. The EBSD detector takes information from the interaction of the electron beam in the SEM and the tilted sample surface ( $\sim 70^\circ$ ), which produce backscattered electrons, that are captured on a phosphorous screen to create Electron Backscatter Diffraction (EBSD) patterns [22]. A schematic of this set up can be seen in Figure 9. EBSD patterns created in an SEM give information that can be used to determine local crystallographic orientation of a sample similar to Kikuchi patterns created in a Transmission Electron Microscope (TEM). EBSD can also determine lattice misorientations and orientation gradients present in deformed material, which is important in understanding the levels of stored energy in the material after deformation [23].

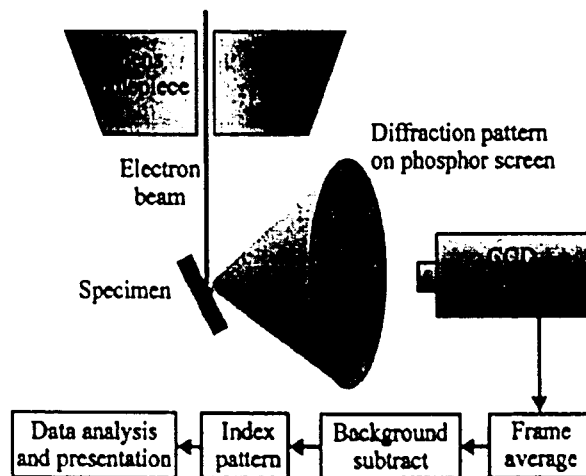
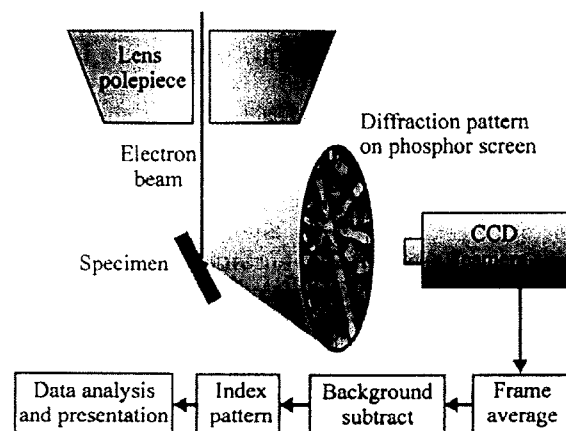


Figure 9. Set up for an electron back scatter diffraction pattern, and the collected Kikuchi pattern<sup>23</sup>



material. To obtain more precise information about recrystallization and texture development during deformation processing it is beneficial to use a Scanning Electron Microscope (SEM) integrated with an Electron Backscatter Diffraction Detector. The EBSD detector takes information from the interaction of the electron beam in the SEM and the tilted sample surface ( $\sim 70^\circ$ ), which produce backscattered electrons, that are captured on a phosphorous screen to create Electron Backscatter Diffraction (EBSD) patterns [22]. A schematic of this set up can be seen in Figure 9. EBSD patterns created in an SEM give information that can be used to determine local crystallographic orientation of a sample similar to Kikuchi patterns created in a Transmission Electron Microscope (TEM). EBSD can also determine lattice misorientations and orientation gradients present in deformed material, which is important in understanding the levels of stored energy in the material after deformation [23].



**Figure 9.** Set up for an electron back scatter diffraction pattern, and the collected Kikuchi pattern<sup>23</sup>

Figure 10 shows a common indexing overlay on an EBSD pattern gathered from a FCC metal. This pattern is able to identify, at a specific point in the sample, what the crystallographic orientation is based on a database of known materials and expected orientations. A major advantage of EBSD over other crystallographic determination techniques, such as TEM and powder diffraction, is that it can determine the orientation for a large number of grains from a bulk sample. Preparation of EBSD samples follows more traditional metallographic techniques, instead of the special preparation needed for TEM samples, which proves to be another advantage of EBSD. Because EBSD is able to map a large number of grains over a sample surface, the relationship between many grains and the corresponding crystallographic texture can be made. For hot deformed FCC materials such as aluminum, the preferred orientation of individual grains can be determined. Because these grains are deformed to large strains, they begin to create a preferred orientation versus a more random orientation distribution associated with the bulk material prior to deformation.

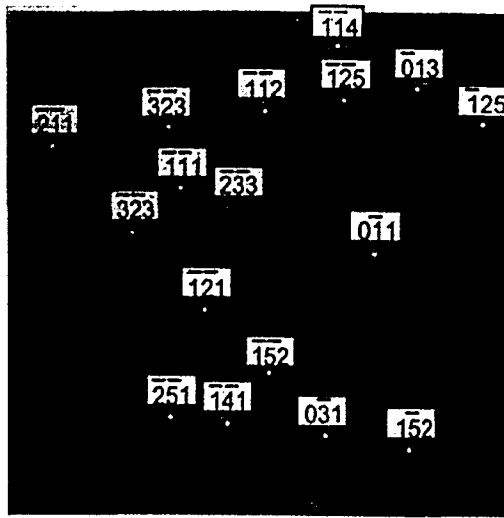


**Figure 10.** An example an EBSD pattern with the indexed crystallographic planes identified<sup>22</sup>

EBSD analysis is also capable of giving information about recrystallization, specifically the percent recrystallized of a material [23]. For microstructures determined by EBSD, deformed grains will show detectable subgrain formation while recrystallized grains will appear to be free of well defined subgrains [24]. Deformation can be characterized by Orientation Image Microscopy (OIM) maps that display information on boundary misorientation and crystallographic texture. This is done by determining misorientations between neighboring pixels throughout an area scan. The most effective way to determine the fraction of recrystallized grains from EBSD is to create a misorientation histogram. This diagram will display the total number fraction of pixel misorientations in degrees throughout the entire scan and plot it versus known misorientations. An example of this type of histogram can be seen in Figure 11.

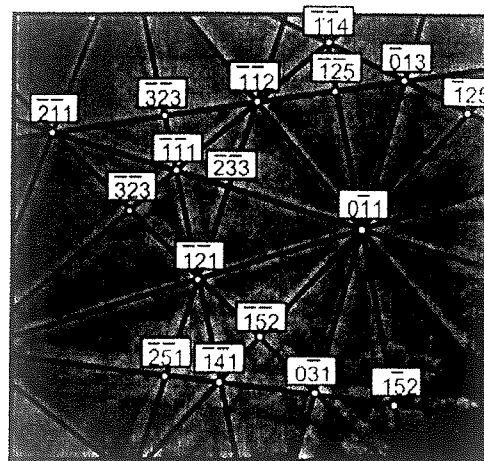
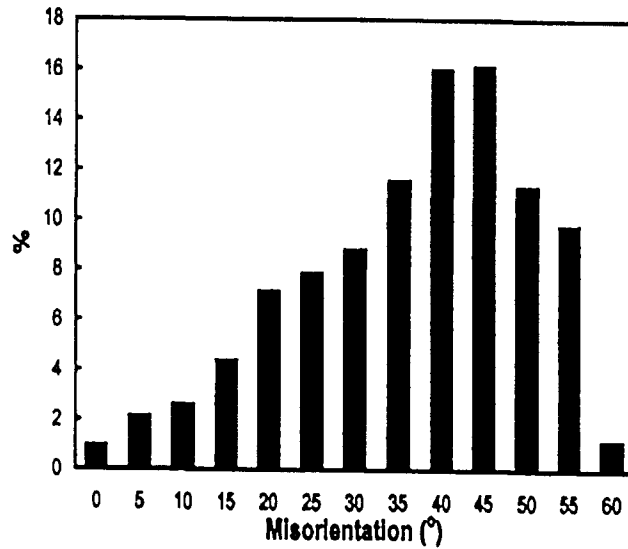


Figure 10. An example an EBSD pattern with the indexed crystallographic planes identified<sup>22</sup>

EBSD analysis is also capable of giving information about recrystallization, specifically the percent recrystallized of a material [23]. For microstructures determined by EBSD, deformed grains will show detectable subgrain formation while recrystallized grains will appear to be free of well defined subgrains [24]. Deformation can be characterized by Orientation Image Microscopy (OIM) maps that display information on boundary misorientation and crystallographic texture. This is done by determining misorientations between neighboring pixels throughout an area scan. The most effective way to determine the fraction of recrystallized grains from EBSD is to create a misorientation histogram. This diagram will display the total number fraction of pixel misorientations in degrees throughout the entire scan and plot it versus known misorientations. An example of this type of histogram can be seen in Figure 11.

For this figure, misorientations greater than  $15^\circ$  are taken to be high angle grain boundaries, while subgrains are represented by misorientations between  $2^\circ - 15^\circ$ . Any remaining deformed grains will be signified by the presence of subgrain boundaries within the parent grain.



**Figure 11.** Misorientation histogram for a material that has a high volume fraction of recrystallized grains. The Y-axis represents the area fraction of recrystallized grains<sup>24</sup>

## 2.0 Procedure

### 2.1 Material

Aluminum alloy 6061 used for these experiments was provided by Alcoa Technical Center with a chemistry within the specifications set by the Aluminum Association. To understand the effects of chromium additions on recrystallization kinetics during annealing, two alloys representing Cr:Mn ratios of 1:1 (Low Cr) and 2:1 (High Cr) were used. The total Cr + Mn levels were 0.17 wt % for the low Cr and 0.35 wt % for the high Cr. Direct Chill (DC) cast billets were homogenized for 3 hours at 555°C (1030°F) in a laboratory furnace, and cooled to room temperature at a cooling rate of 16.8°C/hr. The rolling samples were machined out of the mid-radius of the billet. The mid-radius represents an area of the cast billet where there is a constant average grain size. The shell zone, found at the periphery of the billet, is characterized as showing a non-uniform chemistry which is undesirable. To avoid this area, the samples used for the rolling experiments were sectioned from the mid-radius. Figure 12 shows a schematic representing the area of the billet where the samples were taken from.

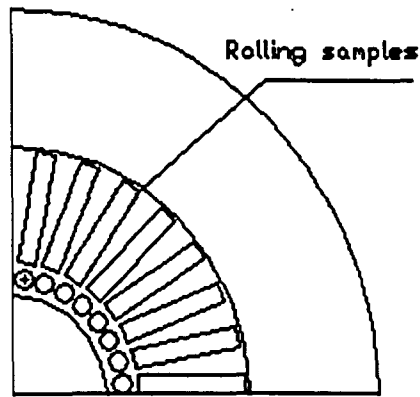


**Figure 12.** Diagram representing the relative area that the rolling samples were sectioned from the DC cast billet

## **2.2 Lab Scale Hot Rolling and Flash Annealing Experiment**

### **2.2.1 Lab Scale Hot Rolling Equipment Set Up**

Laboratory scale hot rolling experiments were performed at Alcoa Technical Center in Monroeville, Pennsylvania. These experiments were conducted using a FENN two-high rolling mill with a 0.15 m (5.875 inch) roll diameter and a speed of 0.20 m/s (40 ft/min). Lubrication was used for the experiments, and the temperature of the rolls was 82°C (180°F). A ceramic block was placed between the work piece and the entry of the rolling press to minimize any heat transfer prior to deformation. Guides were inserted on the table to prevent the rolling samples from deviating from their intended path through the rolls. The size of the rolling work piece prior to deformation was a length of 0.057 m (2.25 inches), width of 0.038 m (1.5 inches) and a thickness of 0.011m (0.4 inches). Thermocouples were attached to the ends of the samples and connected to a data recorder to determine the temperature of the rolling samples before and during

deformation. Recording the temperature of the samples before each rolling pass was critical in understanding the effects of the annealing temperature on the microstructural evolution. A summary of the processing parameters and the sample designations can be seen in Table III. A total of thirteen different processing conditions were examined for this research when taking into account, alloy chemistry, rolling temperature, number of passes, and total reduction. For the multi-pass samples, the roll gap was opened to allow the sample to be pulled back through the rolling mill and reinserted into the furnace to bring the sample back to the desired temperature. Roll speeds were adjusted to prevent any possible curling of the samples during deformation.



**Table III:** Summary of Lab Scale Hot Rolling Conditions and the sample designation

Sample	Alloy	Temp °C	# Passes	Reduction
A	High	482 (900°F)	1	90%
B	High	482 (900°F)	3	90%
C	Low	482 (900°F)	3	90%
D	High	482 (900°F)	3	75%
E	Low	482 (900°F)	3	75%
F	Low	482 (900°F)	1	75%
G	High	482 (900°F)	1	75%
H	High	400 (750°F)	1	75%
I	Low	400 (750°F)	1	75%
J	High	400 (750°F)	3	75%
K	Low	400 (750°F)	3	75%
L	High	400 (750°F)	1	90%
M	Low	400 (750°F)	1	90%

### 2.2.2 Rolling Schedules

Two different rolling schedules were used for this experiment. A single pass and a multi-pass rolling schedule that consisted of three passes to reach the desired reduction were used. The multipass schedule was used because it more closely resembles industrial practice.

For the single pass deformation, the samples were heated just above their desired deformation temperature to account for any radiant heat loss during the

transfer of the material from the furnace to the rolling mill which was approximately 10 – 15 seconds. For the 400°C (750°F) condition, the sample was heated to 410°C (770°F), and for the 482°C (900°F) condition, the sample was heated to 493°C (920°F). For the single pass deformation schedule, the samples were deformed to a total reduction of either 75% or 90% after the preheat. The final sample thickness for the 75% reduction was 2.54 mm (0.1 inches) and 1.02 mm (0.04 inches) for the 90% reduction. Immediately after the material left the rolls, they were water quenched with a forced water spray and then further quenched by submersion in water. This technique was used to insure that the deformed microstructure was preserved as the material left the rolls.

The multi pass rolling schedule consisted of 3 individual reductions with total reductions of either 75% or 90%. The deformation schedule and the related sample thicknesses for the 75% and 90% total reductions can be seen in Table IV and Table V respectively. Similar to the single pass heat treatment prior to deformation, the multi pass samples were also slightly over heated to values of 410°C (770°F) and 493°C (920°F) to account for any heat loss during the transfer of the sample from the furnace to the rolling mill. For the multi pass rolling schedule, there was also interpass annealing that occurred after the first and second passes. After the first and second passes, the samples were placed back in the furnace for a half hour to bring them back up to the desired deformation temperature. A forced water quench was applied to the samples only after the final pass through the rolling mill.

**Table IV: Multi-Pass Rolling Schedule for a 75% Total Reduction**

	Initial	Pass 1	Pass 2	Pass 3
Thickness	10.16 mm (0.4 in.)	8.20 mm (0.32 in.)	3.05 mm (0.12 in.)	2.54 mm (0.1 in.)
Pass Reduction (%)	0	20	62.5	16.7
Total Reduction (%)	0	20	70	75

**Table V: Multi-Pass Rolling Schedule for a 90% Total Reduction**

	Initial	Pass 1	Pass 2	Pass 3
Thickness	10.16 mm (0.4 in.)	8.20 mm (0.32 in.)	3.05 mm (0.12 in.)	1.02 mm (0.04 in.)
Pass Reduction (%)	0	20	62.5	66.7
Total Reduction (%)	0	20	70	90

### 2.2.3 Flash Annealing

After the deformation processing was completed for the thirteen sets of rolling conditions, samples were sectioned from the mid-section of the rolled sheet and subsequently flash annealed in a salt pot at 762°C (912°F). The purpose for using this temperature was to simulate the condition of the work piece just as it is exiting the rolls after deformation. The salt pot annealing experiments took place at Lehigh University in Bethlehem, Pennsylvania. The samples were annealed for 3, 5, 7, and 10 seconds using Liquid Heat 169. After annealing, the samples were immediately water quenched in a water bath. The transfer time from the salt pot to the water bath was less than one second. The flash annealing tests were conducted to examine the recrystallization kinetics during a non-isothermal heat treatment

and also to investigate the surface microstructural evolution during recrystallization of hot rolled aluminum sheet.

## **2.3 Light Optical Microscopy**

### **2.3.1 Sample Preparation**

Rolled samples used for Light Optical Microscopy (LOM) were metallographically prepared for an analysis of the volume percent of recrystallized material. Samples that were sectioned out of the rolled sheet were approximately 0.021 m (0.75 inches) x 0.013 m (0.5 inches). After they were sectioned out of the sheet, the samples were mounted so the normal direct (ND) – rolling direction (RD) plane was being observed (Figure 13). Next, the samples were ground and polished down to a 0.05  $\mu\text{m}$  colloidal silica surface finish. It is important during this step to obtain a clean surface finish, minimizing scratches, so the etching procedure brings up the best possible microstructure. The samples were electrolytically etched at 30 V for 5 minutes using a modified Barker's reagent and an aluminum cathode. The modified Barker's reagent consisted of 217 mL distilled water, 7.5 mL of  $\text{HBF}_4$ , and 75 mL of Hydrogen Peroxide.

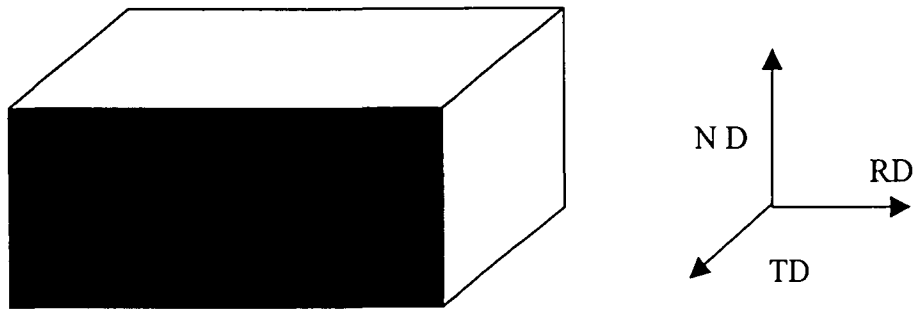


**Figure 13.** The sample orientation for LOM and EBSD analysis. The shaded surface represents the area that was used for analysis.

### **2.3.2 Microstructural Characterization**

Micrographs were taken with an Olympus BH-2 Light Optical Microscope (LOM) using polarized light to analyze the microstructure. The microscope was interfaced with a PAXcam digital camera and PAX-it ver. 6.4 digital imaging software to capture and record the LOM micrographs. The reason that digital imaging was used in this experiment, instead of more traditional film photography, was because it allowed for the creation of collaged images, which require the combination of several smaller digital pictures. The collaged images made it possible to create an image of the entire thickness of the sample, at higher magnification, that would have been more difficult to do with more traditional methods. Finally, the polarized LOM images were analyzed to determine the volume percent of recrystallized grains present at various flash annealing times using the ASTM E 562 point count method. A total of sixty-three micrographs

were analyzed to determine the recrystallization kinetics for the various processing conditions and flash annealing times.

## **2.4 Electron Back Scatter Diffraction (EBSD)**

### **2.4.1 Sample Preparation**

The samples that were prepared for EBSD analysis were polished to a 0.05  $\mu\text{m}$  colloidal silica finish. For an EBSD analysis, it is critical to remove any deformation that may have been introduced on the polished surface during preparation, because this deformation can often lead to a weak back scatter electron signal and therefore poor EBSD patterns. To remove any surface deformation created during mechanical polishing, a chemical polish was applied to the samples within an hour before the EBSD analysis. The chemical polish consisted of 70%  $\text{H}_3\text{PO}_4$  (Phosphoric Acid), 25%  $\text{H}_2\text{SO}_4$  (Sulfuric Acid), and 5%  $\text{HNO}_3$  (Nitric Acid). This solution was heated to approximately 85°C and the samples were submerged for 20 seconds. After the chemical polishing, a clean aluminum background is created with intermetallics raised on the surface. It is important to obtain a good chemical polish on these samples to improve the results of the EBSD analysis.

### **2.4.2 Microstructural Characterization**

EBSD analysis was only performed on four of the thirteen total processing conditions and three of the annealing times: 3, 5, and 7 seconds. These four

conditions exhibited partial recrystallization and therefore would be important in understanding the microstructural evolution through the thickness of the sample. As-deformed and 10 second annealing time samples were excluded because it was concluded from the LOM study that the as deformed samples showed no recrystallization and the 10 second annealed samples showed a completely recrystallized structure. Therefore these sets of annealing conditions were not critical to the EBSD analysis. Table VI shows the four processing conditions chosen for EBSD analysis. EBSD was performed using an EDAX/TSL Digiview Digital Camera interfaced with a Philips XL-30 Environmental Scanning Electron Microscope that was equipped with a tungsten filament.

**Table VI:** Processing Conditions for EBSD Analysis Samples

Sample	Cr Level	Processing Temp (°C)	Number of Passes	Percent Reduction (%)
H	High	400 (750°F)	1	75
I	Low	400 (750°F)	1	75
L	High	400 (750°F)	1	90
M	Low	400 (750°F)	1	90

For each of the four processing conditions and subsequent flash annealing times of 3, 5, and 7 seconds, two EBSD scans were taken. One scan was taken at the surface of the sample and the other was taken from the sample center. The purpose of obtaining these two scans at the surface and in the center of the sample was to gain valuable information about any differences in microstructural evolution at the surface and center of the deformed material. Figure 14 shows a schematic of where the two scans were taken on each sample.

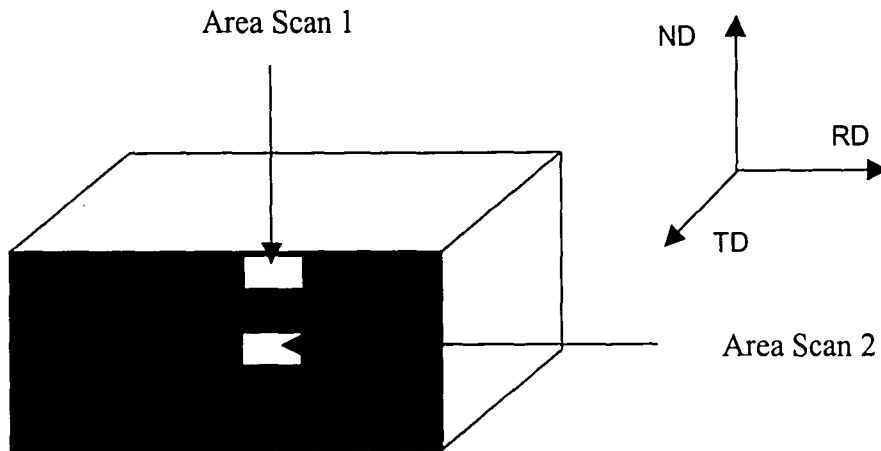


**Figure 14.** The relative position of the two EBSD area scans taken for each sample.

Each area scan was taken at a magnification of 250X. The accelerating voltage was 20 kV, the spot size was 4.5, and the filament current was between 80 – 90 nA. The EBSD software used for this analysis was OIM 3.0. This software gives the operator information about crystallographic texture, Euler angles, image quality, and confidence intervals for each point taken along the area scan. The step size for an area scan can be adjusted through the OIM software; for this set of experiments the step size was 1  $\mu\text{m}$ . A smaller step size creates a finer scanning resolution. This resolution is important because the information gathered about subgrain structure within deformed grains is dependant on the relationship between step size and average subgrain size. After the data was collected, it was “cleaned” by the OIM 3.0 software. This data clean up function works by assigning a texture value to each point taken during the scan based on its confidence index. If the confidence index for a given point is below a minimum



value, the program will assign that point a texture value based on data points surrounding it.

## **3.0 Results**

### **3.1 Light Optical Microscopy**

#### **3.1.1 Deformed and Annealed Microstructures**

It is important to examine the entire thickness of the hot rolled sample to understand the effects of a non-uniform strain gradient. Figures 15 -22 show 8 of 13 total processing conditions with varying rolling temperature, total reduction, Cr content and single or multi pass rolling. All of these figures depict the through thickness microstructure in the transverse plane. These LOM images were later used to determine the fraction recrystallized at various times of 3, 5, 7, and 10 seconds for a flash annealing temperature of 489°C (912°F).

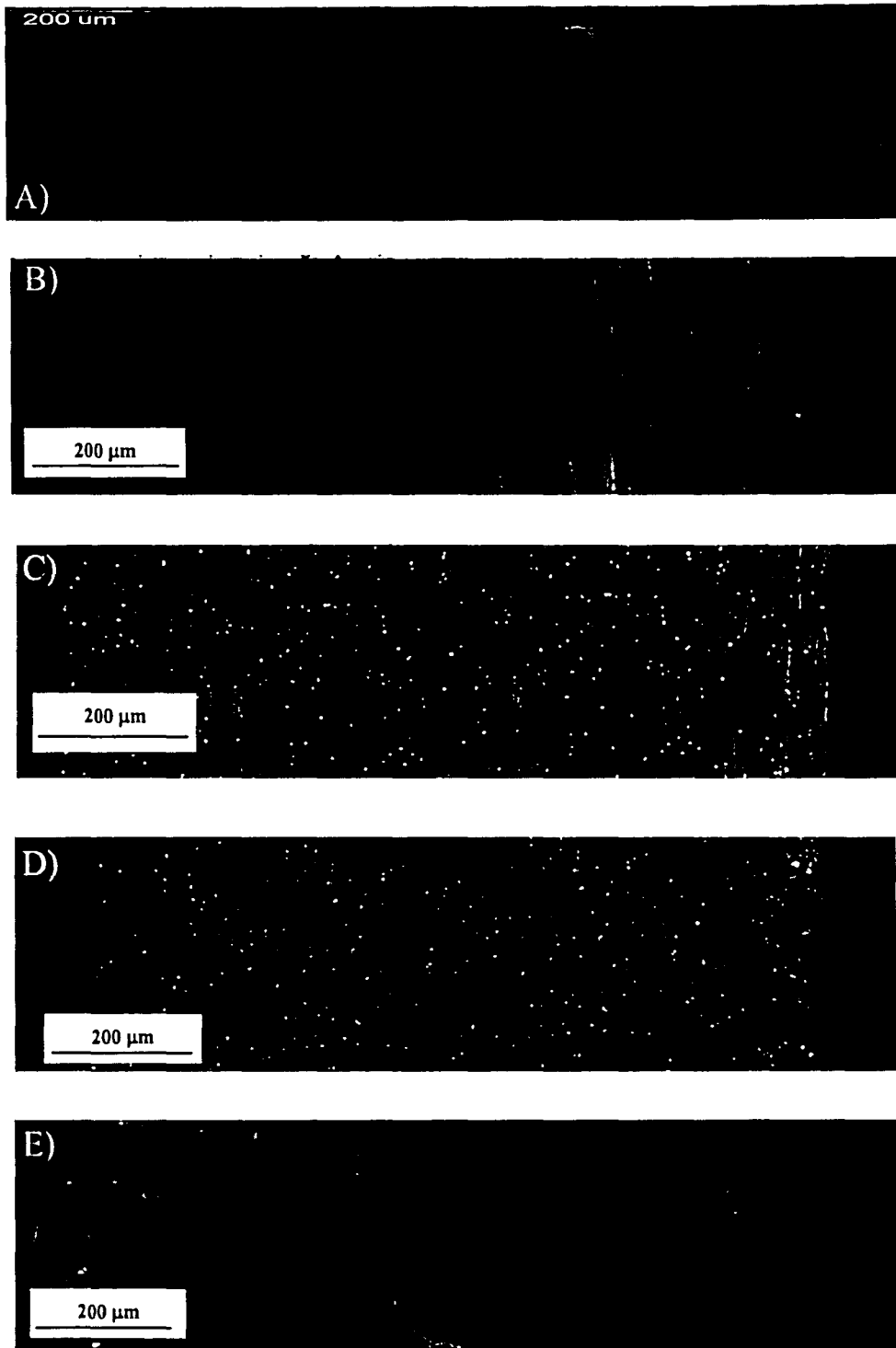


**Figure 15.** Processing Conditions Set A: High Cr content, rolling temperature of 482°C Single Pass, 90% total reduction. A) As Deformed, B) 3 second anneal, C) 5 second anneal, D) 7 second anneal, E) 10 second anneal

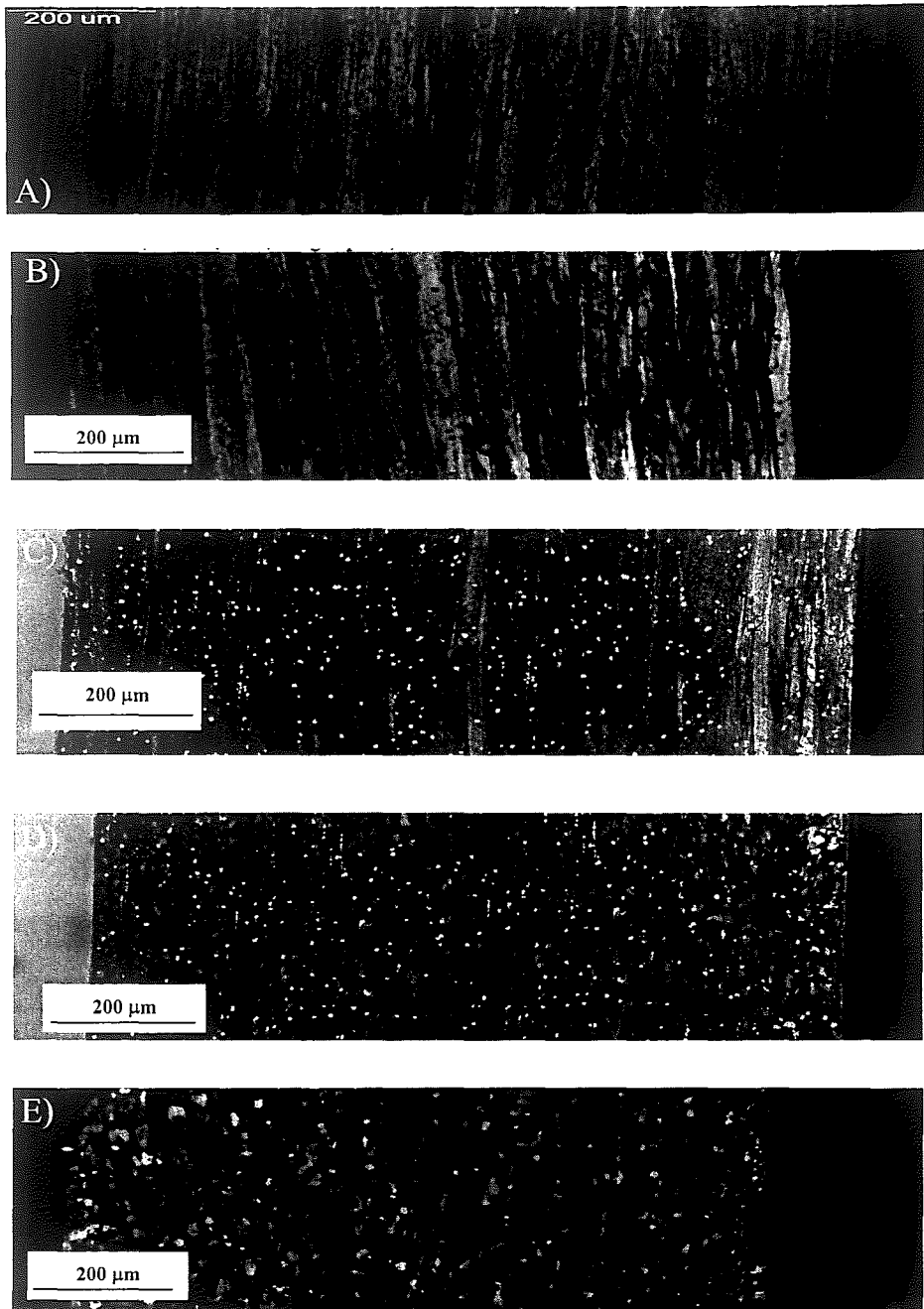


Figure 15. Processing Conditions Set A: High Cr content, rolling temperature of 482°C Single Pass, 90% total reduction. A) As Deformed, B) 3 second anneal, C) 5 second anneal, D) 7 second anneal, E) 10 second anneal

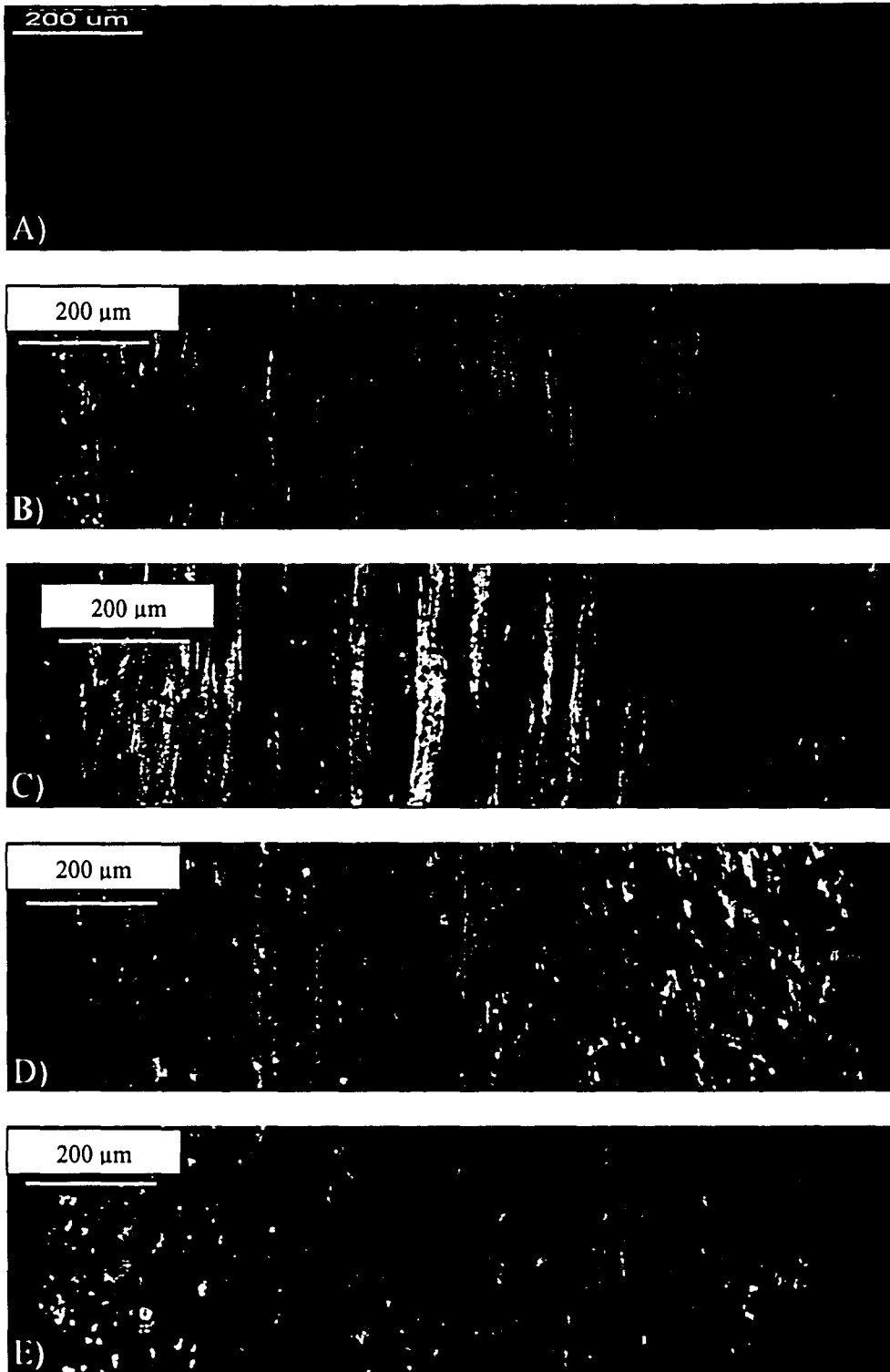


Figure 16. Processing Conditions Set B: High Cr content, rolling temperature of 482°C, 3 Pass, 90% total reduction. A) As Deformed, B) 3 second anneal, C) 5 second anneal, D) 7 second anneal, E) 10 second anneal

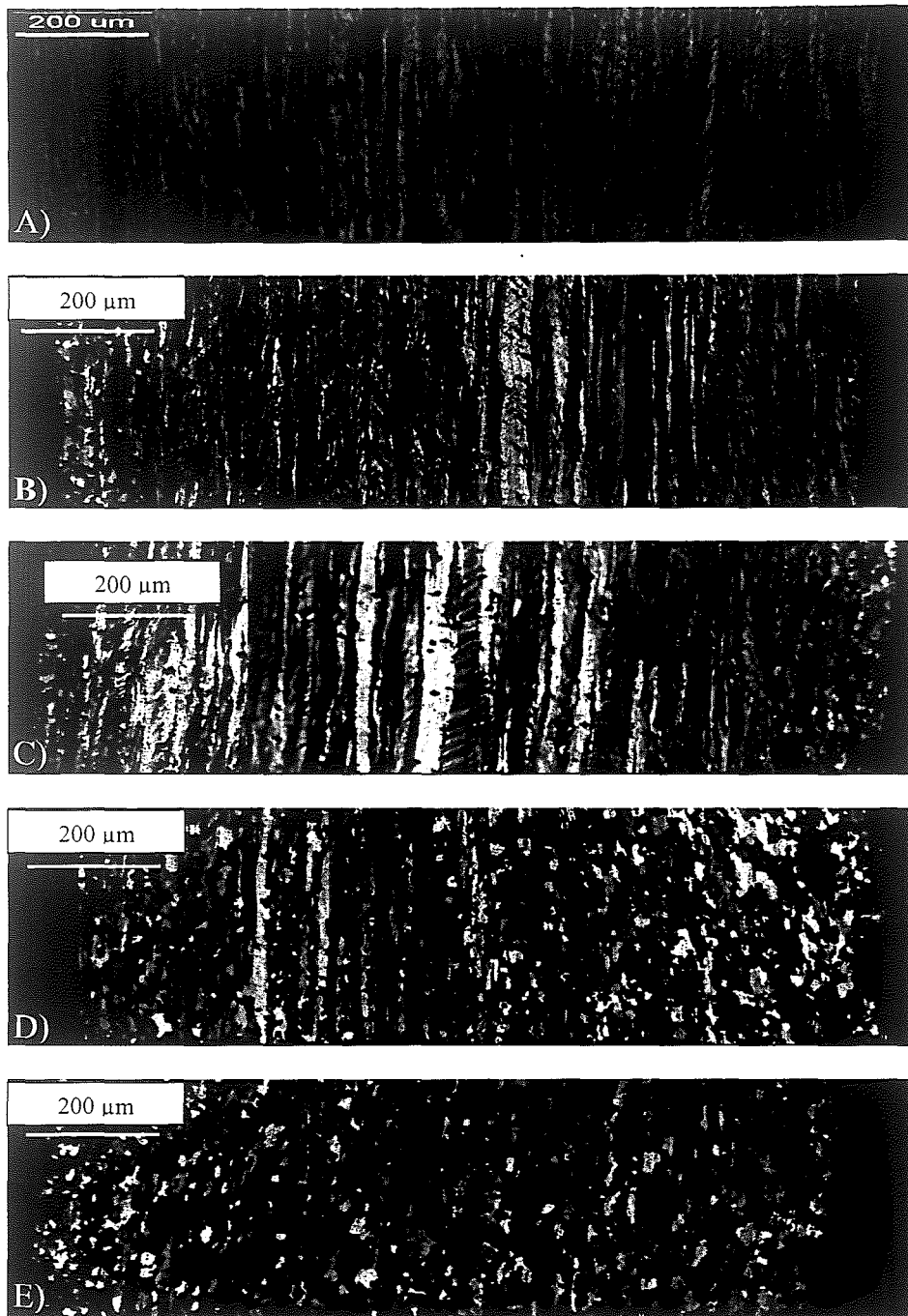


Figure 16. Processing Conditions Set B: High Cr content, rolling temperature of 482°C, 3 Pass, 90% total reduction. A) As Deformed, B) 3 second anneal, C) 5 second anneal, D) 7 second anneal, E) 10 second anneal

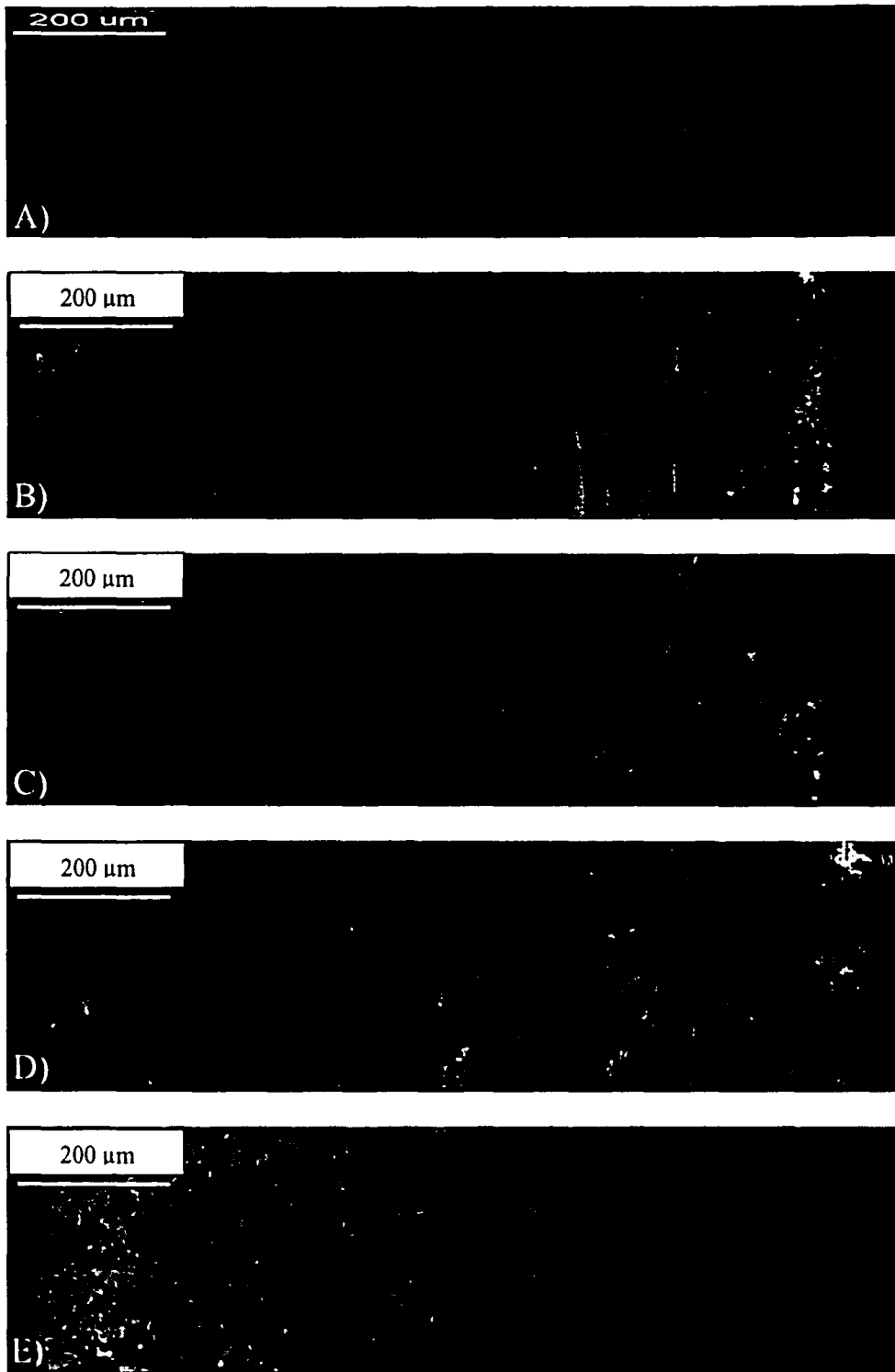
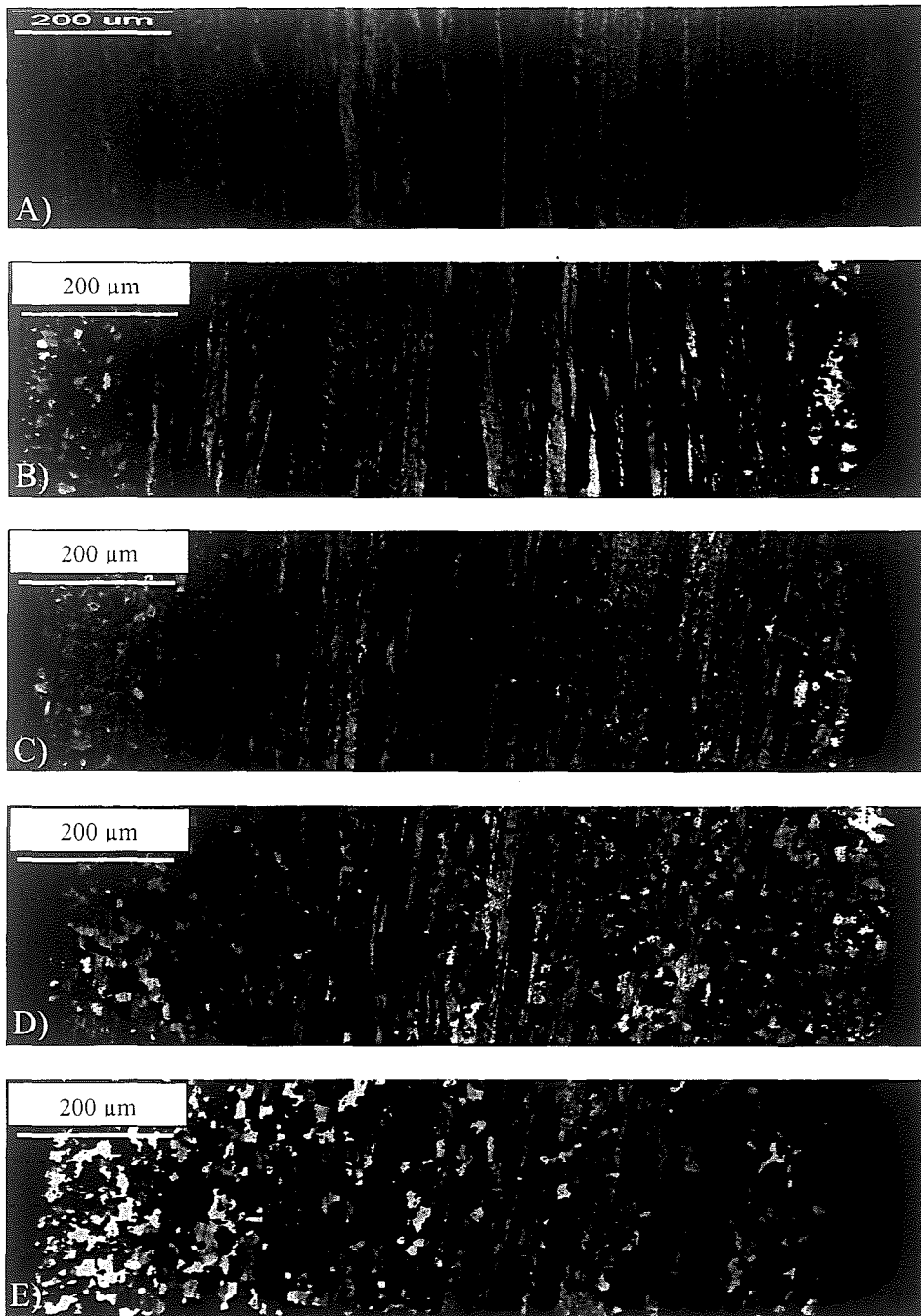
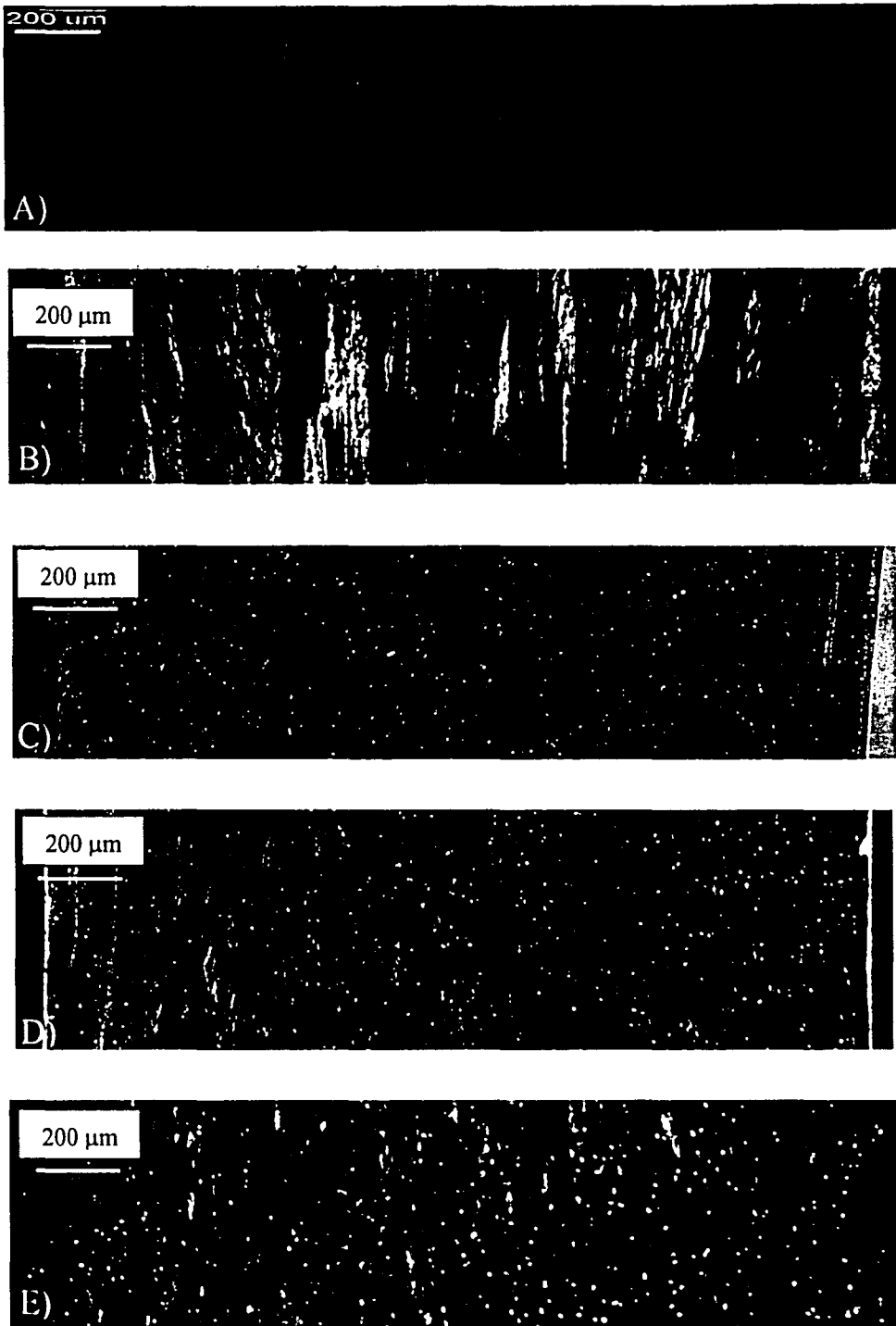


Figure 17. Processing Conditions Set C: Low Cr content, rolling temperature of 482°C, 3 Pass, 90% total reduction. A) As Deformed, B) 3 second anneal, C) 5 second anneal, D) 7 second anneal, E) 10 second anneal



**Figure 17.** Processing Conditions Set C: Low Cr content, rolling temperature of 482°C, 3 Pass, 90% total reduction. A) As Deformed, B) 3 second anneal, C) 5 second anneal, D) 7 second anneal, E) 10 second anneal





**Figure 18.** Processing Conditions Set F: Low Cr content, rolling temperature of 482°C, 1 Pass, 75% total reduction. A) As Deformed, B) 3 second anneal, C) 5 second anneal, D) 7 second anneal, E) 10 second anneal

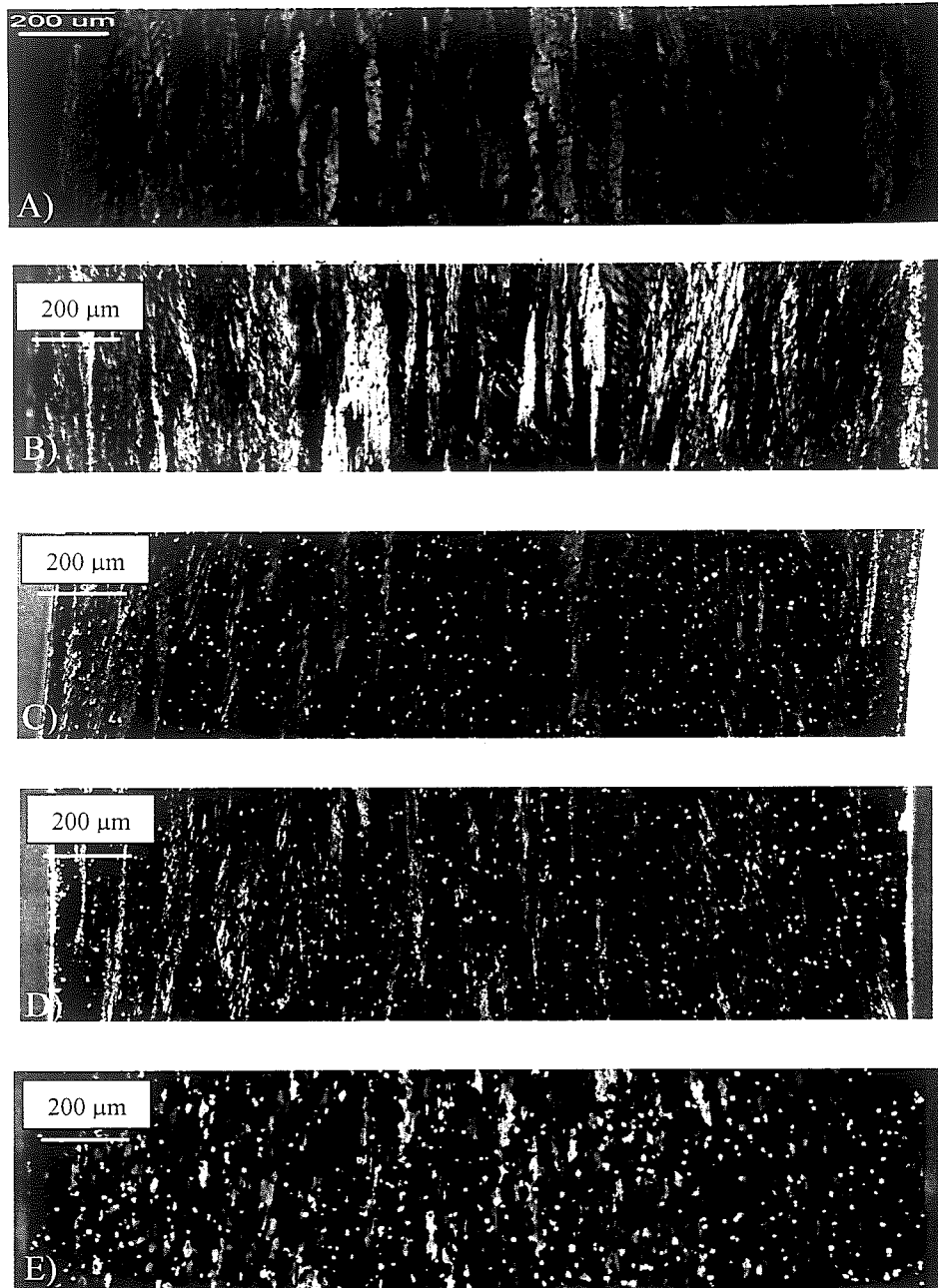
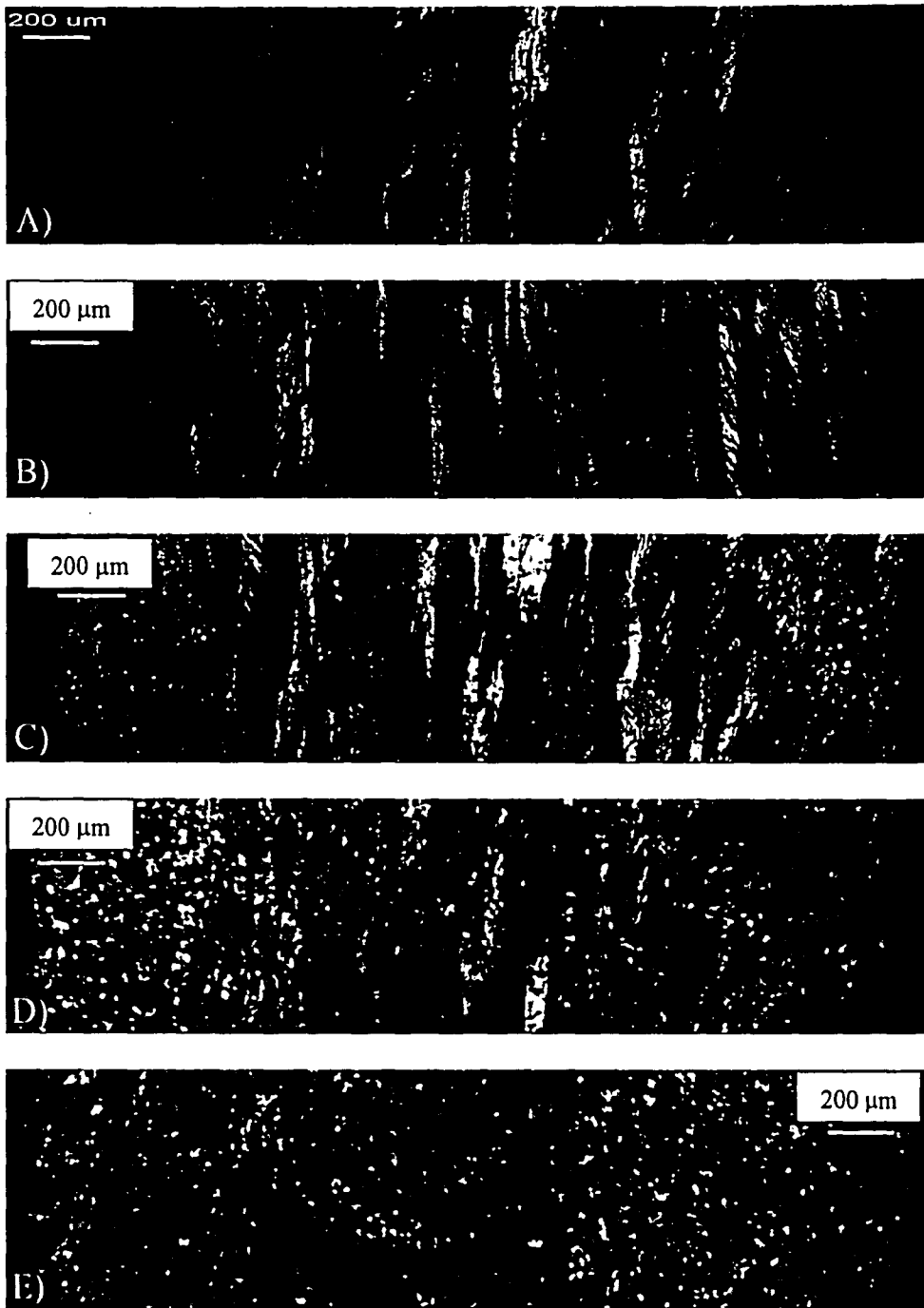


Figure 18. Processing Conditions Set F: Low Cr content, rolling temperature of 482°C, 1 Pass, 75% total reduction. A) As Deformed, B) 3 second anneal, C) 5 second anneal, D) 7 second anneal, E) 10 second anneal



**Figure 19.** Processing Conditions Set H: High Cr content, rolling temperature of 400°C, 1 Pass, 75% total reduction. A) As Deformed, B) 3 second anneal, C) 5 second anneal, D) 7 second anneal, E) 10 second anneal

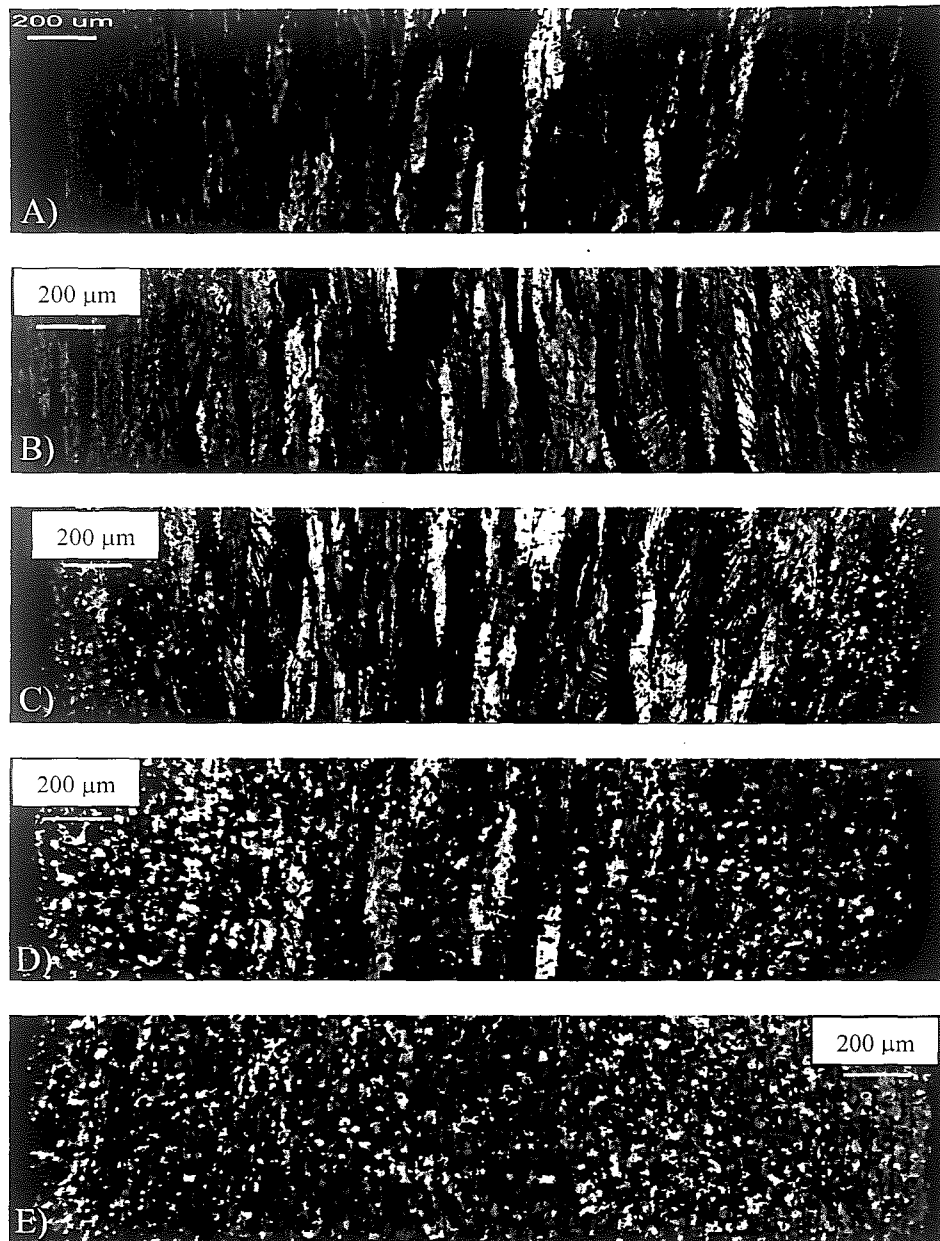
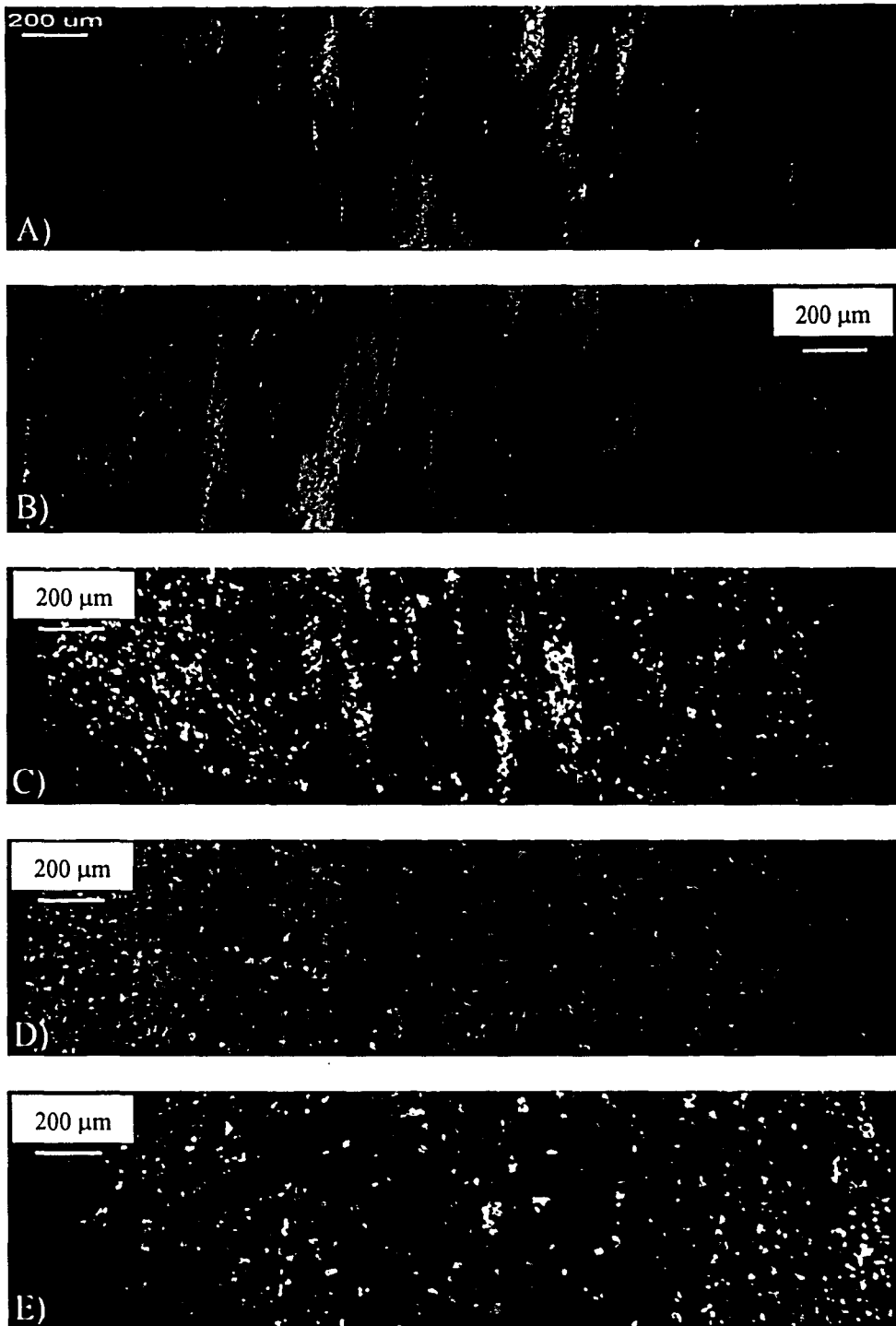


Figure 19. Processing Conditions Set H: High Cr content, rolling temperature of 400°C, 1 Pass, 75% total reduction. A) As Deformed, B) 3 second anneal, C) 5 second anneal, D) 7 second anneal, E) 10 second anneal



**Figure 20.** Processing Conditions Set I: Low Cr content, rolling temperature of 400°C, 1 Pass, 75% total reduction. A) As Deformed, B) 3 second anneal, C) 5 second anneal, D) 7 second anneal, E) 10 second anneal

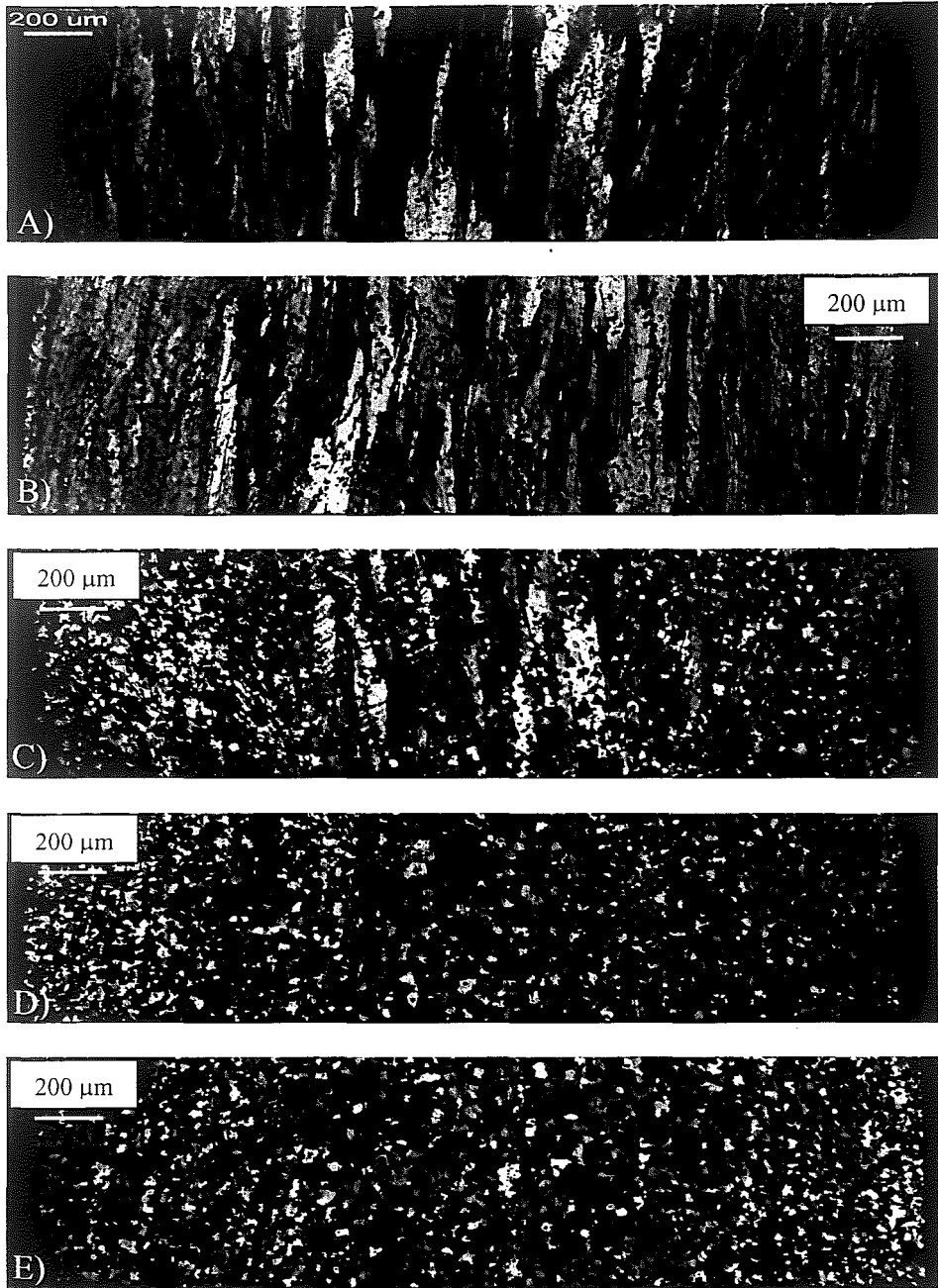


Figure 20. Processing Conditions Set I: Low Cr content, rolling temperature of 400°C, 1 Pass, 75% total reduction. A) As Deformed, B) 3 second anneal, C) 5 second anneal, D) 7 second anneal, E) 10 second anneal

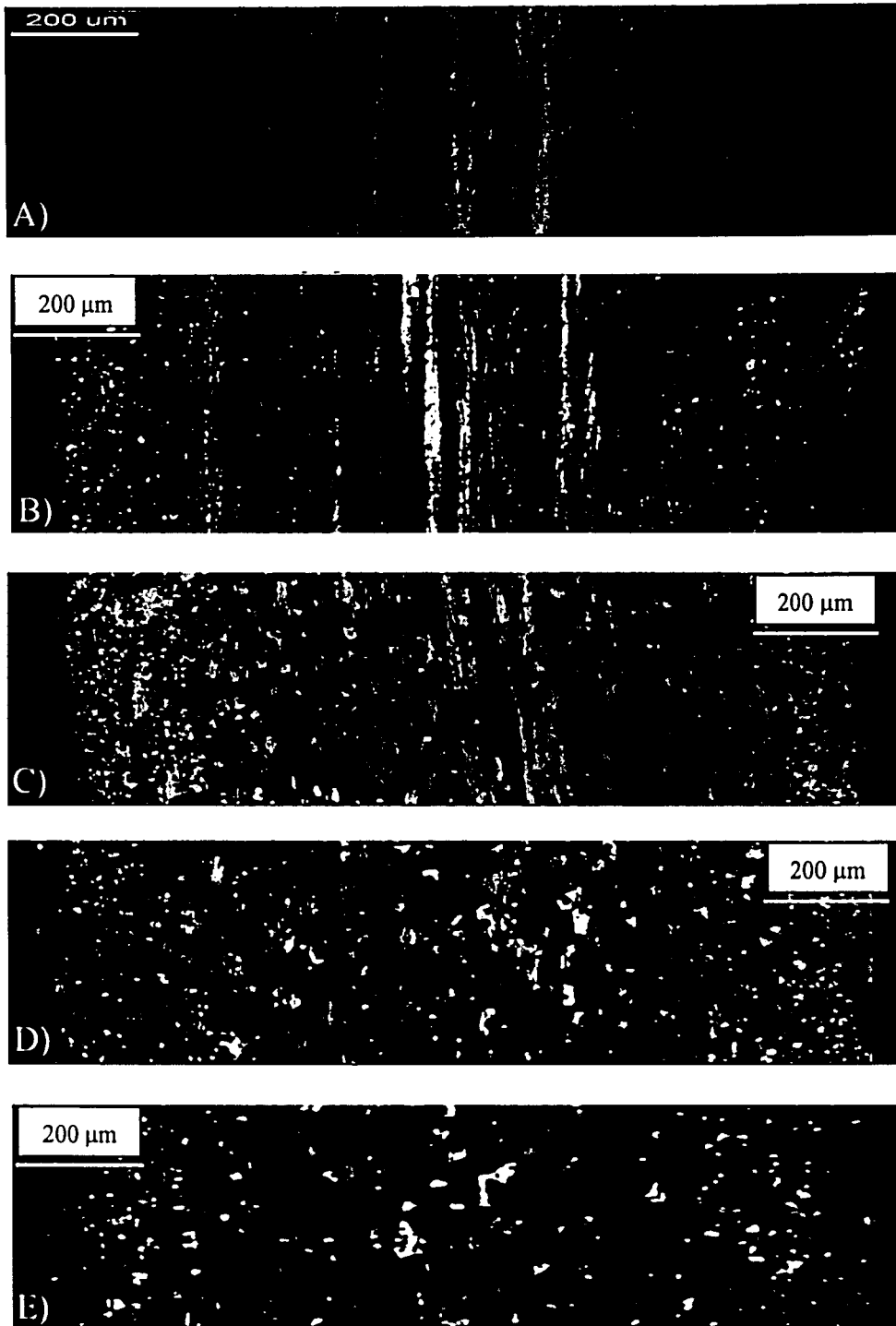


Figure 21. Processing Conditions Set L: High Cr content, rolling temperature of 400°C, 1 Pass, 90% total reduction. A) As Deformed, B) 3 second anneal, C) 5 second anneal, D) 7 second anneal, E) 10 second anneal

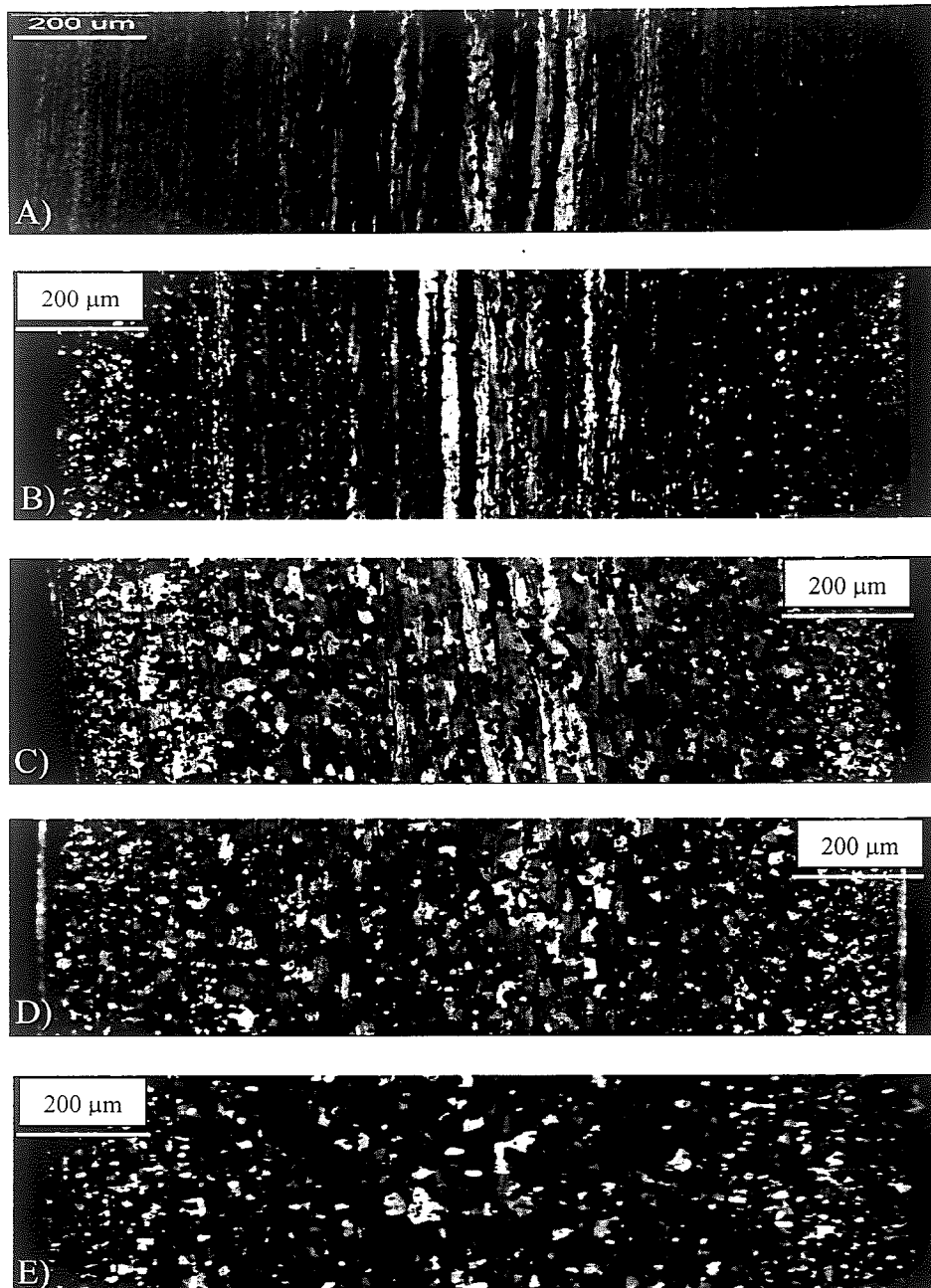
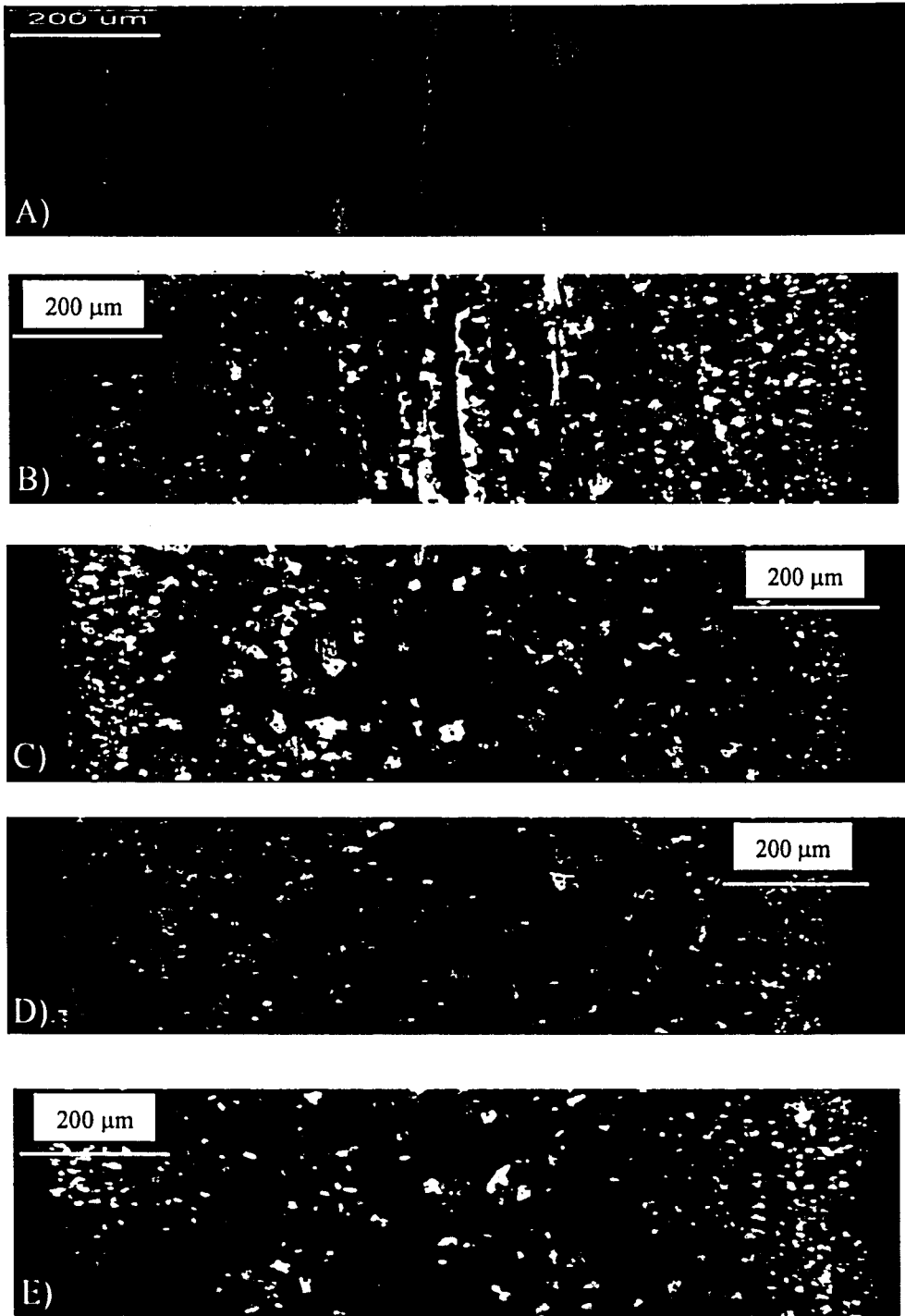
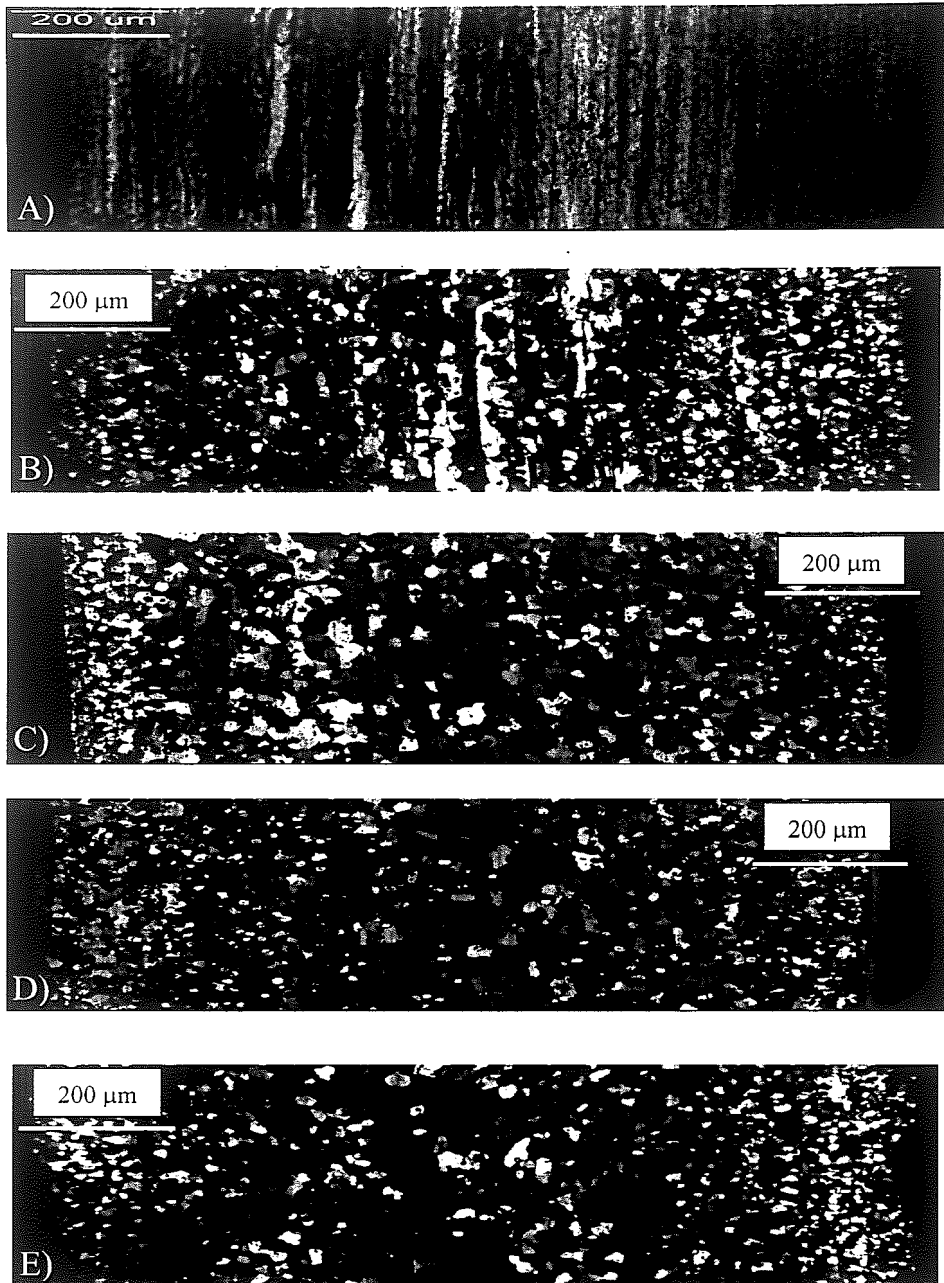


Figure 21. Processing Conditions Set L: High Cr content, rolling temperature of 400°C, 1 Pass, 90% total reduction. A) As Deformed, B) 3 second anneal, C) 5 second anneal, D) 7 second anneal, E) 10 second anneal





**Figure 22.** Processing Conditions Set M: Low Cr content, rolling temperature of 400°C, 1 Pass, 90% total reduction. A) As Deformed, B) 3 second anneal, C) 5 second anneal, D) 7 second anneal, E) 10 second anneal



**Figure 22.** Processing Conditions Set M: Low Cr content, rolling temperature of 400°C, 1 Pass, 90% total reduction. A) As Deformed, B) 3 second anneal, C) 5 second anneal, D) 7 second anneal, E) 10 second anneal

### 3.1.2 Recrystallization Kinetics

Polarized light optical microscopy showed a variation in fraction of recrystallized material versus the flash annealing time. Using the ASTM E 562 standard for the point count method, the volume fraction of recrystallized grains were recorded and can be seen in Table VII. Data presented in this table describes, for each of the processing conditions and flash annealing times, the volume percent of recrystallized grains present.

**Table VII:** Chart showing the volume fraction of recrystallized grains present after various flash annealing times for various processing conditions.

Processing Conditions	Time (sec)				
	0	3	5	7	10
A	0%	0%	5%	95%	100%
B	0%	0%	20%	70%	100%
C	0%	10%	20%	70%	90%
D	0%	0%	10%	10%	30%
E	0%	0%	20%	30%	50%
F	0%	0%	10%	20%	50%
G	0%	0%	10%	40%	100%
H	0%	0%	30%	80%	100%
I	0%	5%	75%	95%	100%
J	0%	0%	5%	20%	100%
K	0%	0%	10%	30%	100%
L	0%	30%	80%	95%	100%
M	0%	80%	95%	100%	100%

From the data set in Table VII relationships can be created to graphically show the difference in recrystallization rate for various variables such as Cr content, rolling temperature, number of rolling passes, and total reduction. Figures 23 – 28 show

graphs comparing the effects of these processing parameters on the kinetics associated with recrystallization during flash annealing.

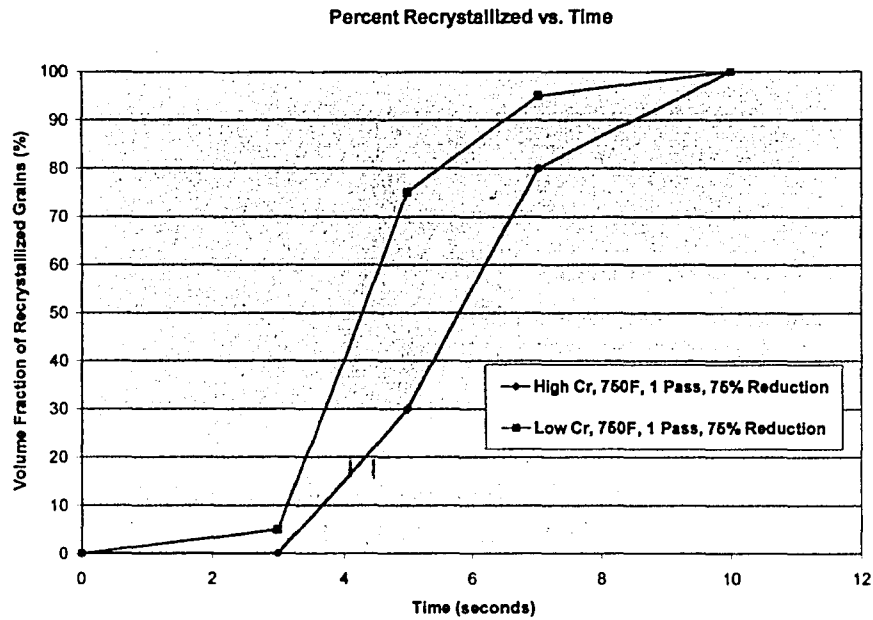


**Figure 23.** Volume fraction of recrystallized grains versus time with high and low Cr levels for a single pass reduction of 75% at 400°C (750°F)

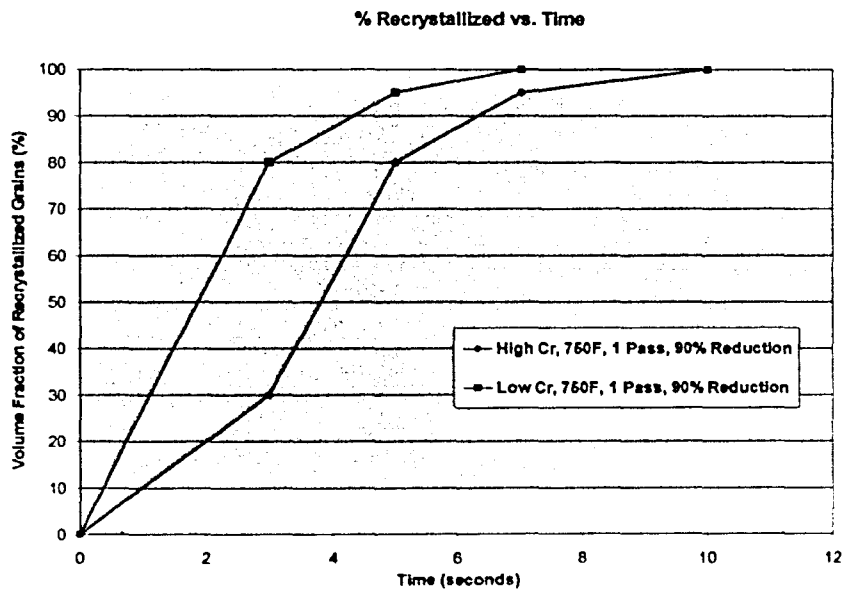


**Figure 24.** Volume fraction of recrystallized grains versus time with high and low Cr levels for a single pass reduction of 90% at 400°C (750°F)

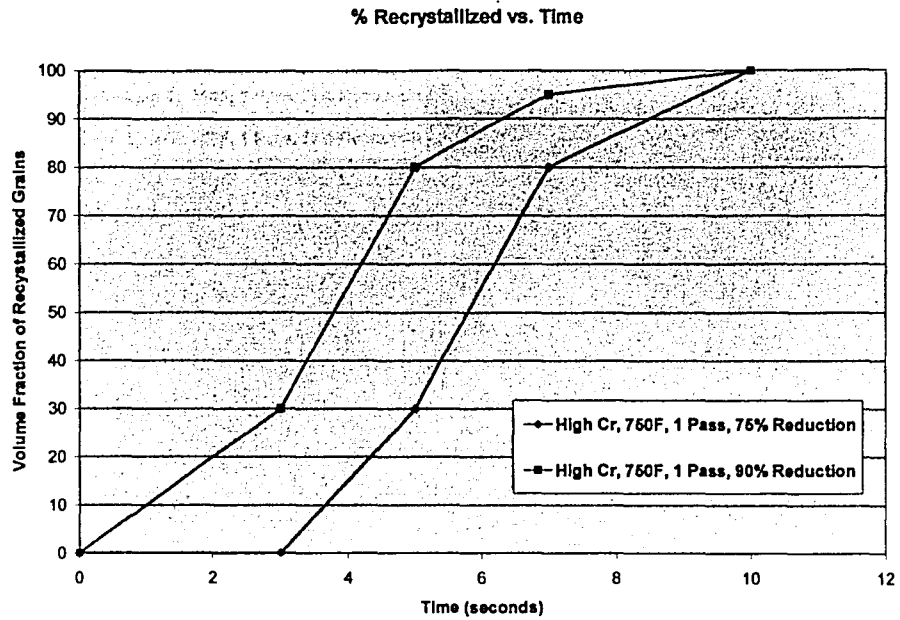


**Figure 25.** Volume fraction of recrystallized grains versus time with 75% and 90% reductions for a high Cr alloy hot rolled with one pass at 400°C (750°F)

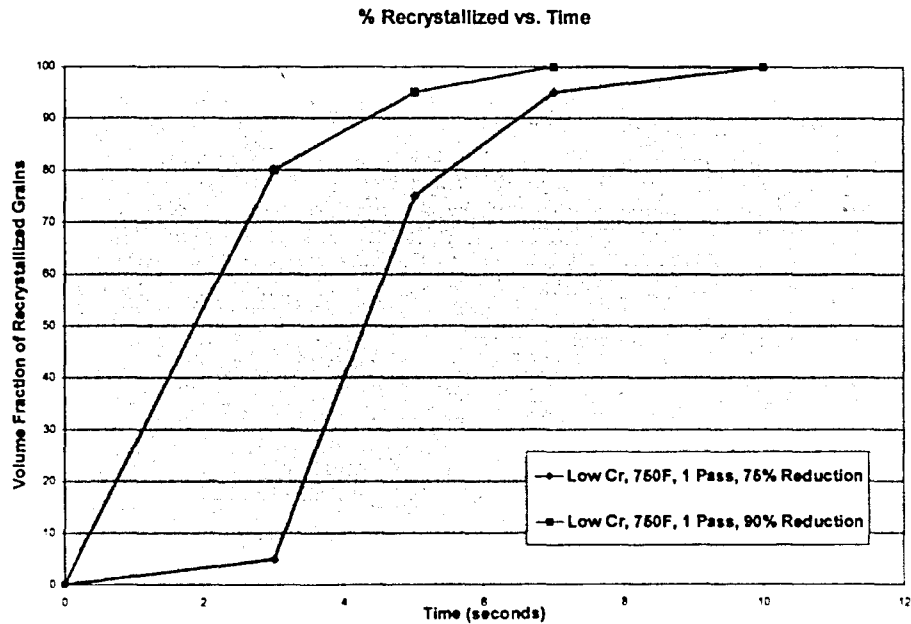


**Figure 26:** Volume fraction of recrystallized grains versus time with 75% and 90% reductions for a low Cr alloy hot rolled with one pass at (400°C) 750°F

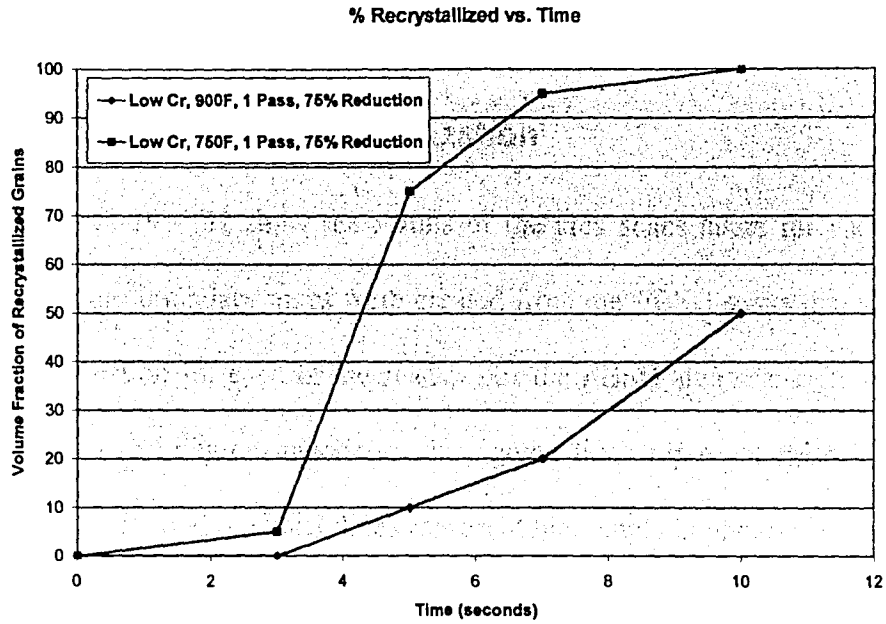


**Figure 27:** Volume fraction of recrystallized grains versus time for deformation temperatures of 400°C (750°F) and 482°C (900°F) reductions for a low Cr alloy hot rolled with one pass to a 75% reduction

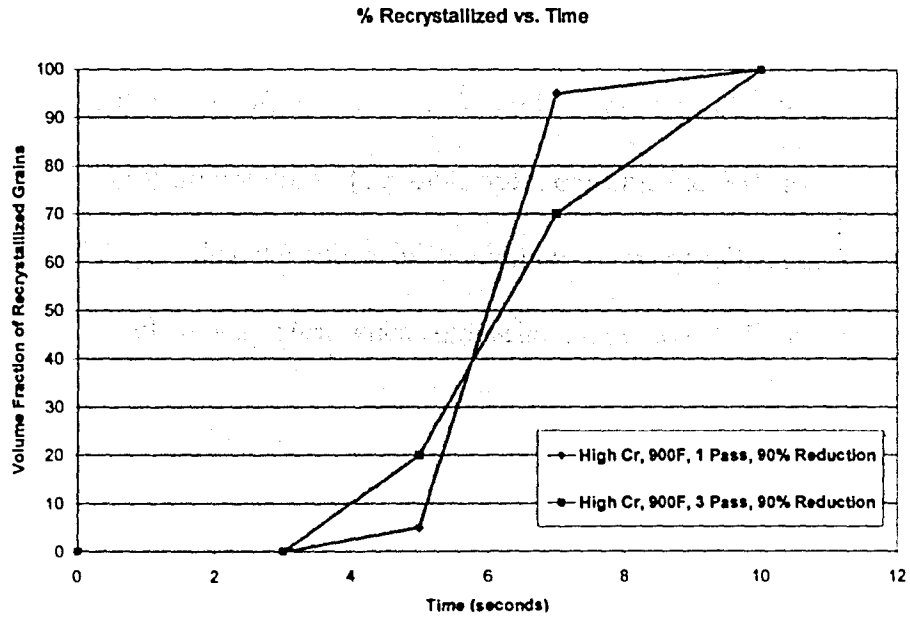
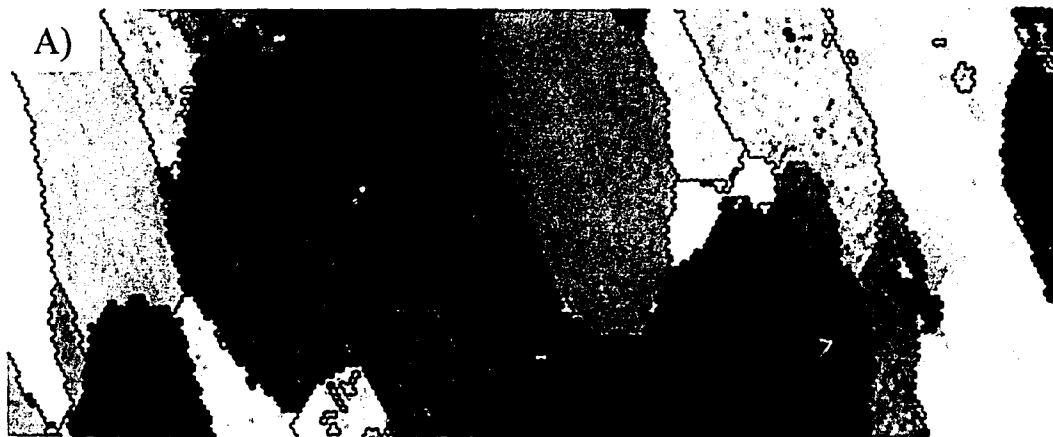


**Figure 28:** Volume fraction of recrystallized grains versus time for single pass versus multi pass deformation to a total reduction of 90% at 482°C (900°F) with a high Cr content

## 3.2 Electron Backscatter Diffraction

### 3.2.1 Microstructural Characterization

Figures 29 – 32 show the results of the area scans taken for each of the samples. Grain boundary maps were created from the EBSD scans that show the subgrain formation for each of the scans. For the EBSD area scans the red lines represent  $1^\circ - 5^\circ$  degree misorientations, green lines represent misorientations between  $5^\circ - 15^\circ$ , and the black lines represent high angle boundaries greater than  $15^\circ$  misorientations. Figures 29 and 30 show the difference in recrystallization at the surface and center after a five second anneal for a sample deformed under identical conditions. Figure 30B shows the presence of deformed grains mixed with recrystallized grains after the 5 second anneal. The deformed grains are represented with a black arrow. Figures 31 and 32 show the effects of Cr content on the recrystallization of the surface of samples deformed to 90% in a single pass at  $400^\circ\text{C}$  ( $750^\circ\text{F}$ ). Also, the effects of Cr additions on recrystallization kinetics on the localized level are very clear when comparing Figure 31B to Figure 32B.



40.00  $\mu\text{m}$  = 40 steps    Boundary levels: 15°  
IPF [001]



40.00  $\mu\text{m}$  = 40 steps    Boundary levels: 1° 5° 15°  
IQ 41...224.9

**Figure 29.** EBSD area scan for a sample with low Cr content, rolled to a 75% reduction in a single pass at 400°C (750°F) taken at the sample surface after a 5 second anneal. A) Inverse Pole Figure Map, B) Grain Boundary Map.



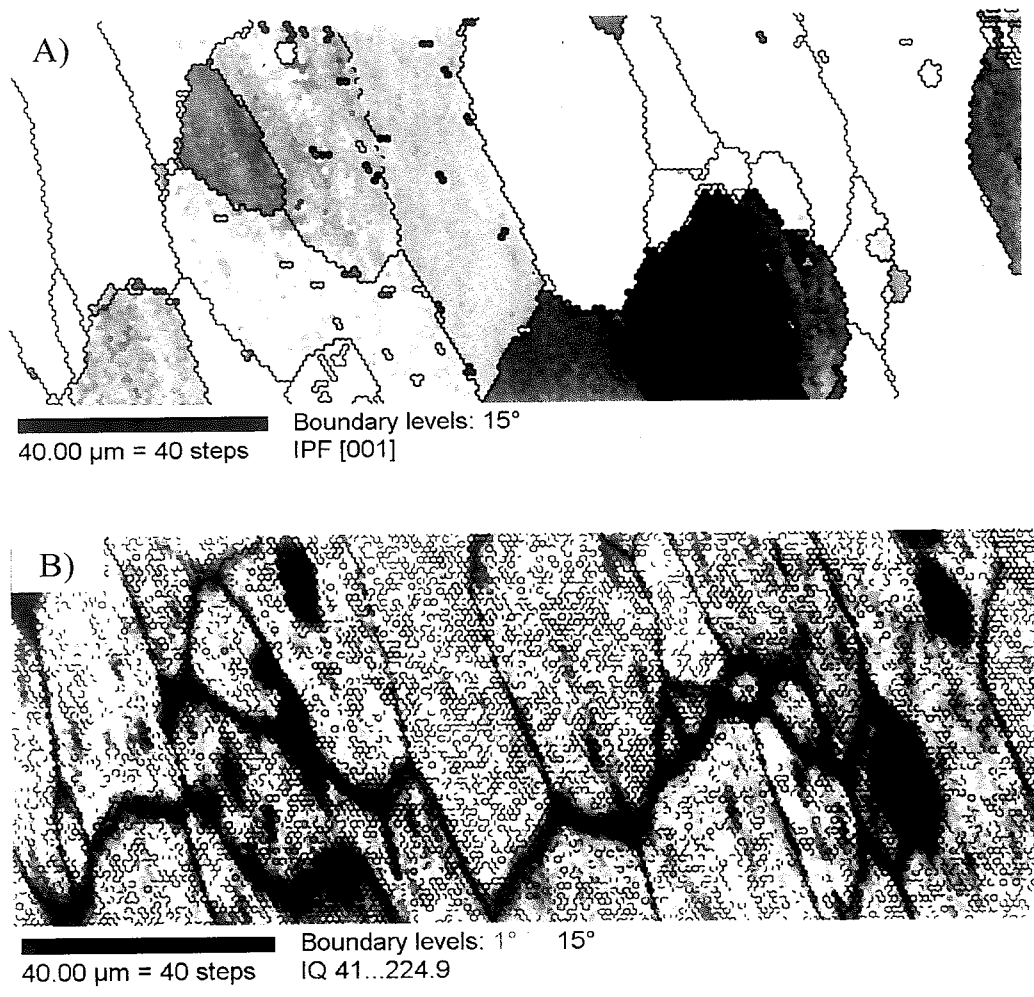


**Figure 29.** EBSD area scan for a sample with low Cr content, rolled to a 75% reduction in a single pass at 400°C (750°F) taken at the sample surface after a 5 second anneal. A) Inverse Pole Figure Map, B) Grain Boundary Map.

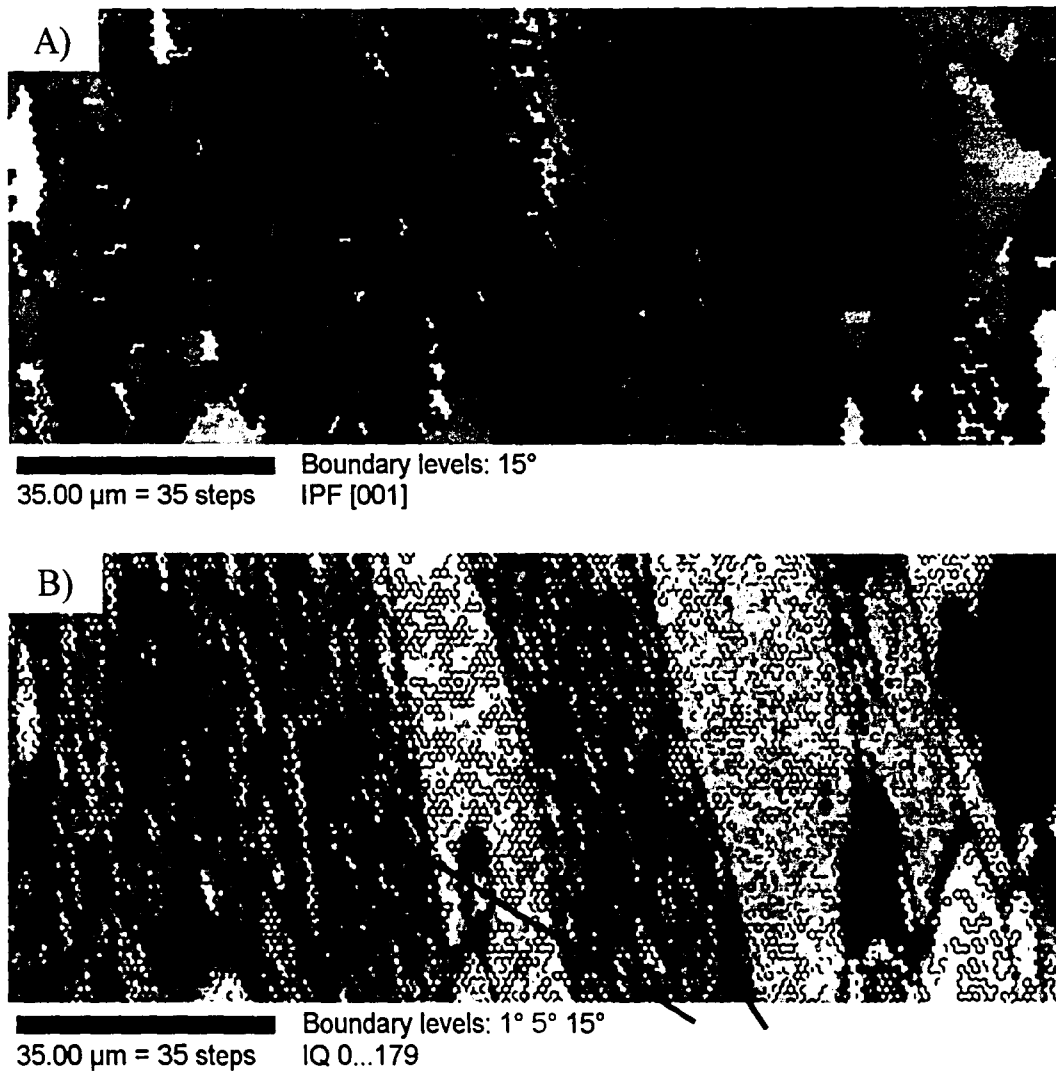


**Figure 30.** EBSD area scan for a sample with low Cr content, rolled to a 75% reduction in a single pass at 400°C (750°F) taken at the sample center after a 5 second anneal. A) Inverse Pole Figure Map, B) Grain Boundary Map. The black arrows mark areas of deformed material.

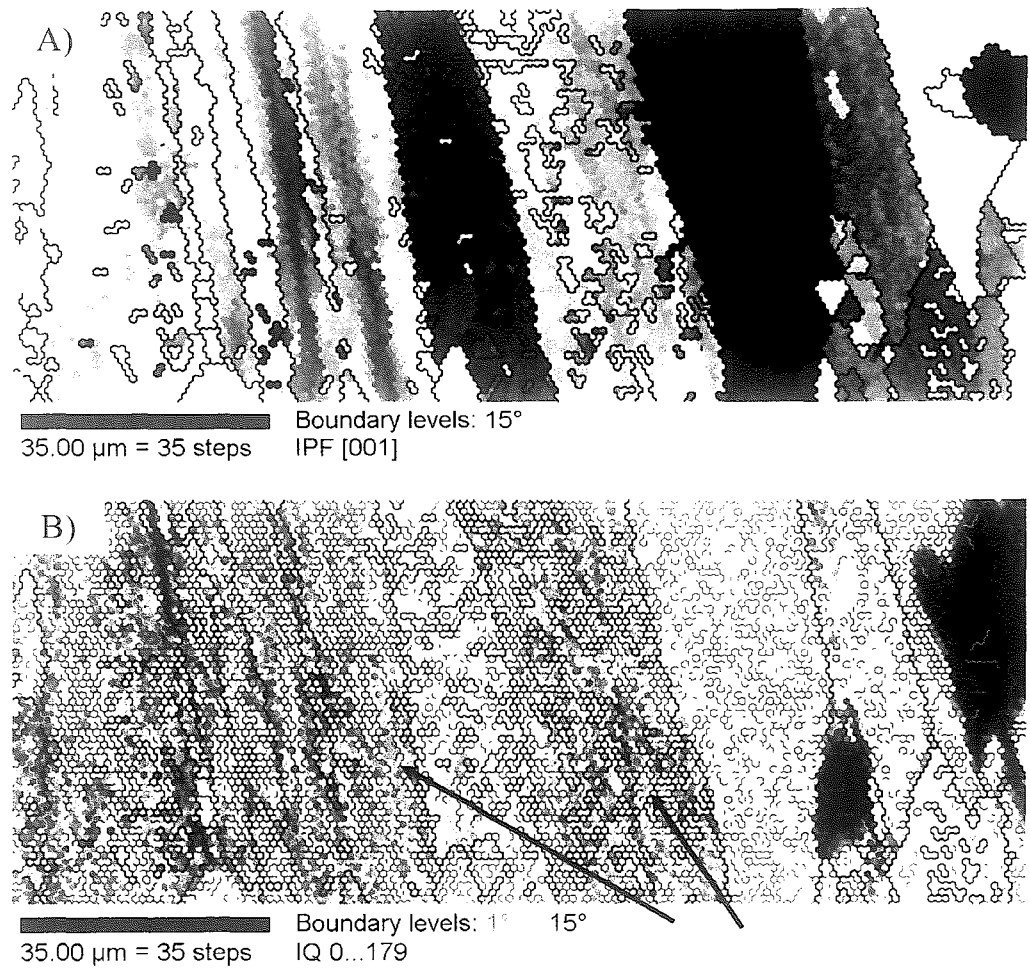
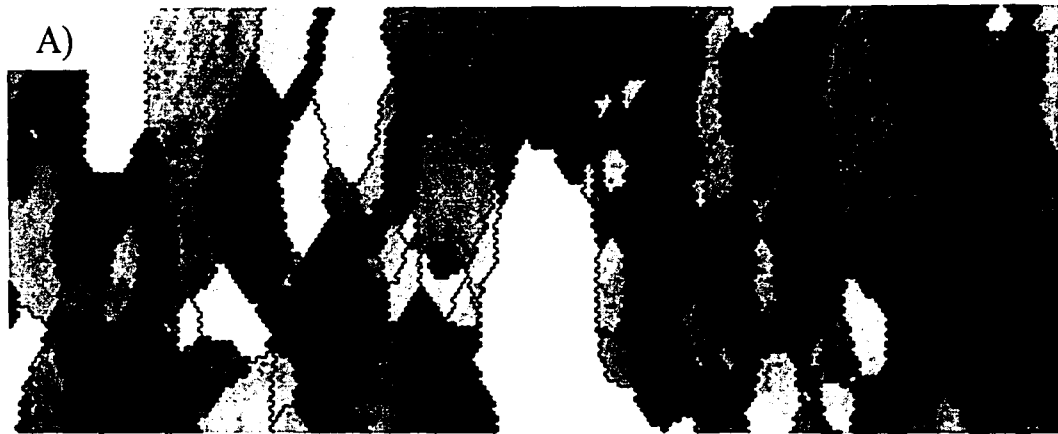


**Figure 30.** EBSD area scan for a sample with low Cr content, rolled to a 75% reduction in a single pass at 400°C (750°F) taken at the sample center after a 5 second anneal. A) Inverse Pole Figure Map, B) Grain Boundary Map. The black arrows mark areas of deformed material.



40.00  $\mu\text{m}$  = 40 steps      Boundary levels: 15°  
IPF [001]



40.00  $\mu\text{m}$  = 40 steps      Boundary levels: 1° 5° 15°  
IQ 39.2...197.1

**Figure 31.** EBSD area scan for a sample with low Cr content, rolled to a 90% reduction in a single pass at 400°C (750°F) taken at the sample surface after a 3 second anneal. A) Inverse Pole Figure Map, B) Grain Boundary Map.

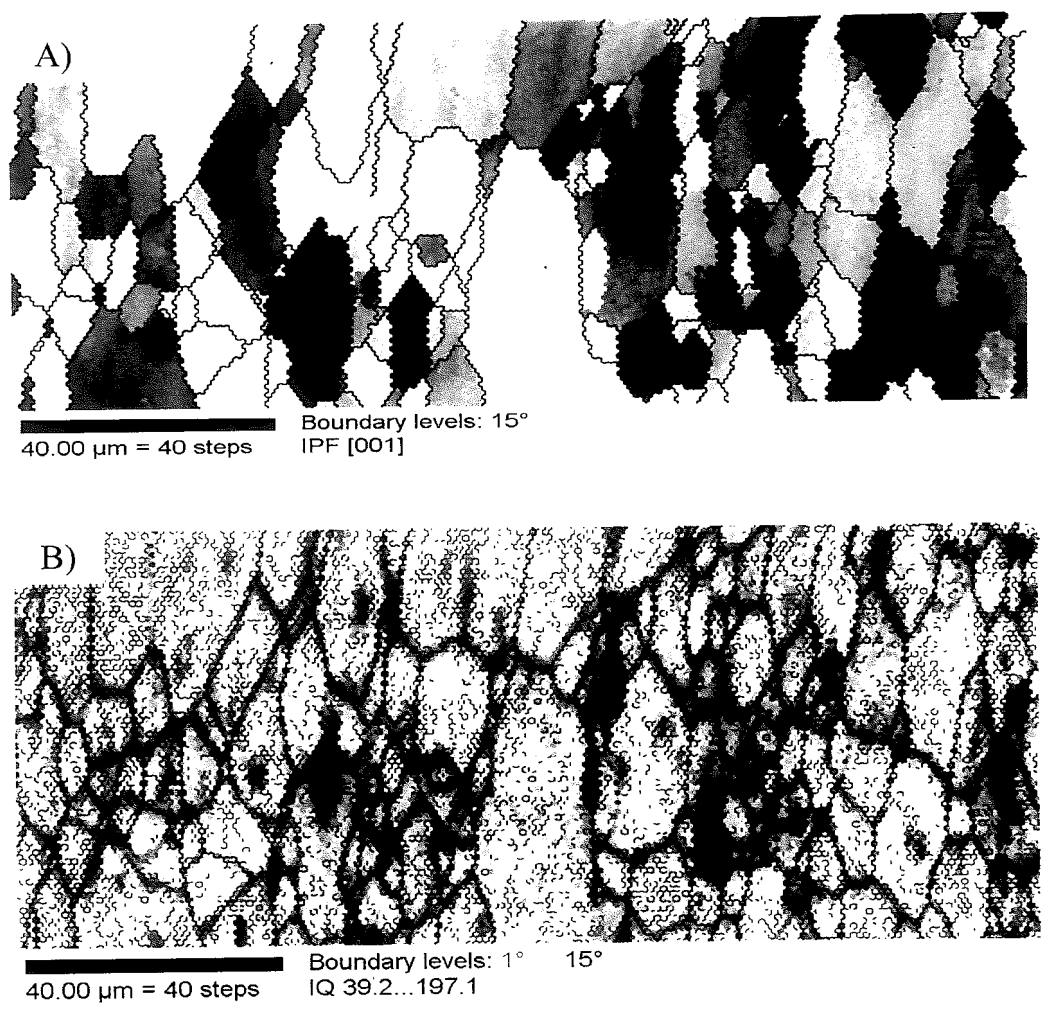
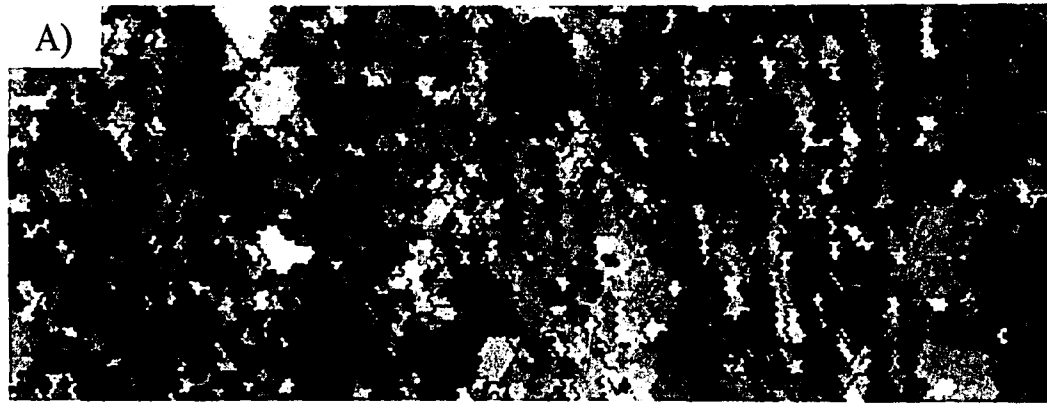
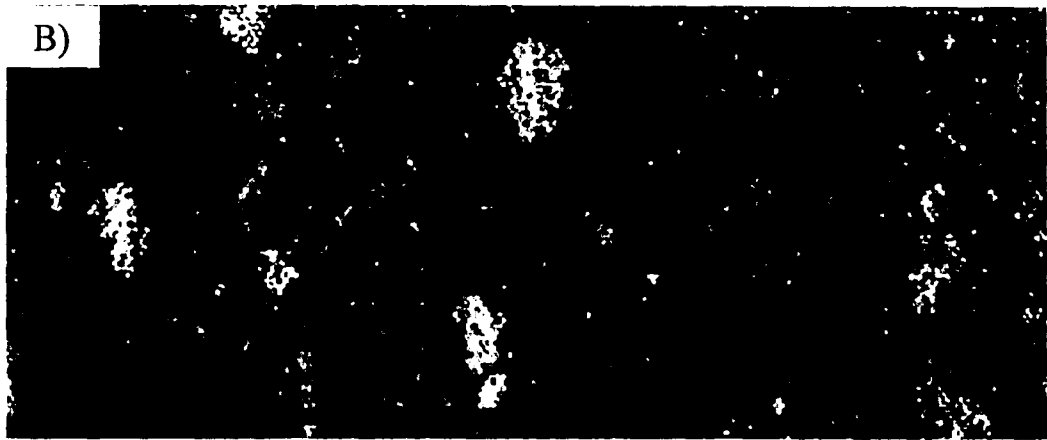


**Figure 31.** EBSD area scan for a sample with low Cr content, rolled to a 90% reduction in a single pass at 400°C (750°F) taken at the sample surface after a 3 second anneal. A) Inverse Pole Figure Map, B) Grain Boundary Map.



35.00  $\mu\text{m}$  = 35 steps    Boundary levels: 15°  
IPF [001]



35.00  $\mu\text{m}$  = 35 steps    Boundary levels: 1° 5° 15°  
IQ 21.9...188.7

**Figure 32.** EBSD area scan for a sample with high Cr content, rolled to a 90% reduction in a single pass at 400°C (750°F) taken at the sample surface after a 3 second anneal. A) Inverse Pole Figure Map, B) Grain Boundary Map. The black arrows point to areas of recrystallized material.

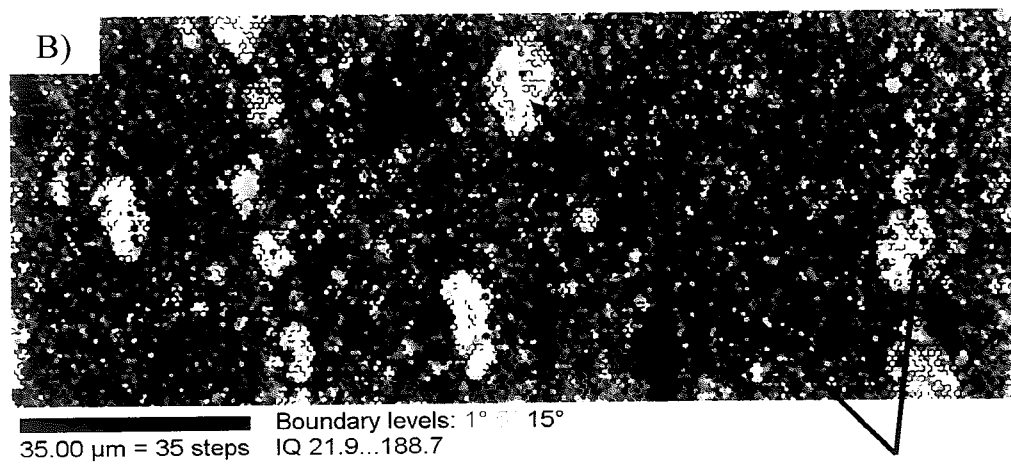
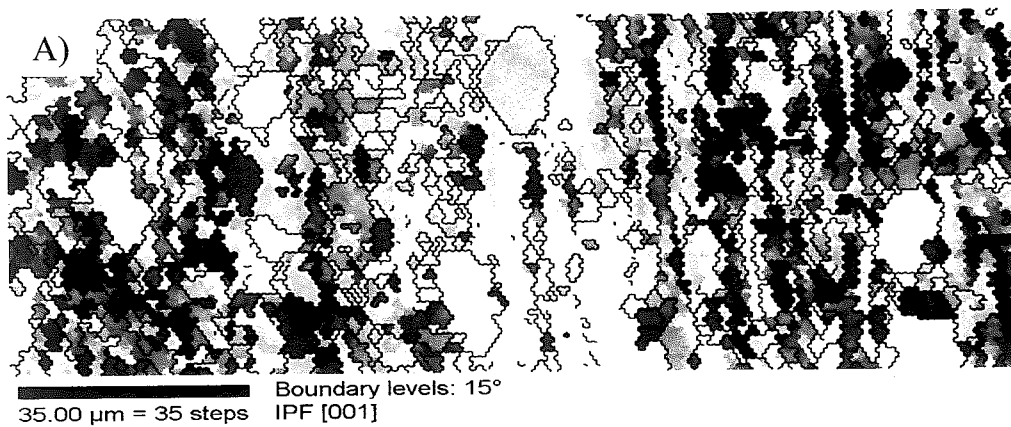


**Figure 32.** EBSD area scan for a sample with high Cr content, rolled to a 90% reduction in a single pass at 400°C (750°F) taken at the sample surface after a 3 second anneal. A) Inverse Pole Figure Map, B) Grain Boundary Map. The black arrows point to areas of recrystallized material.

### 3.2.2 Non-Uniform Recrystallization Kinetics

Using EBSD area scans at the surface and the center of four sets of processing conditions (H, I, L, M) misorientation histograms were created to examine the recrystallization kinetics. Figure 33 show the progression of misorientation versus number fraction histograms for the H series samples taken at the surface. The values for percent recrystallized at annealing times of 0 and 10 seconds were assumed to be 0% and 100% recrystallized respectively from LOM results. Table VIII shows the results for percent recrystallized at the surface and center for each of the four processing conditions. Figures 34 – 37 compare the kinetics of recrystallization at the center and the surface for each of the processing conditions.

**Table VIII:** Volume Fraction of recrystallized grains at the center and surface for four processing conditions exhibiting differences in kinetics at the surface versus the center of the strip thickness

Processing Condition	Time (s)			
	3	5	7	10
H Surface	48%	60%	90%	100%
H Center	30%	54%	92%	100%
I Surface	42%	81%	90%	100%
I Center	37%	71%	93%	100%
L Surface	63%	86%	93%	100%
L Center	41%	45%	95%	100%
M Surface	85%	89%	92%	100%
M Center	87%	90%	92%	100%



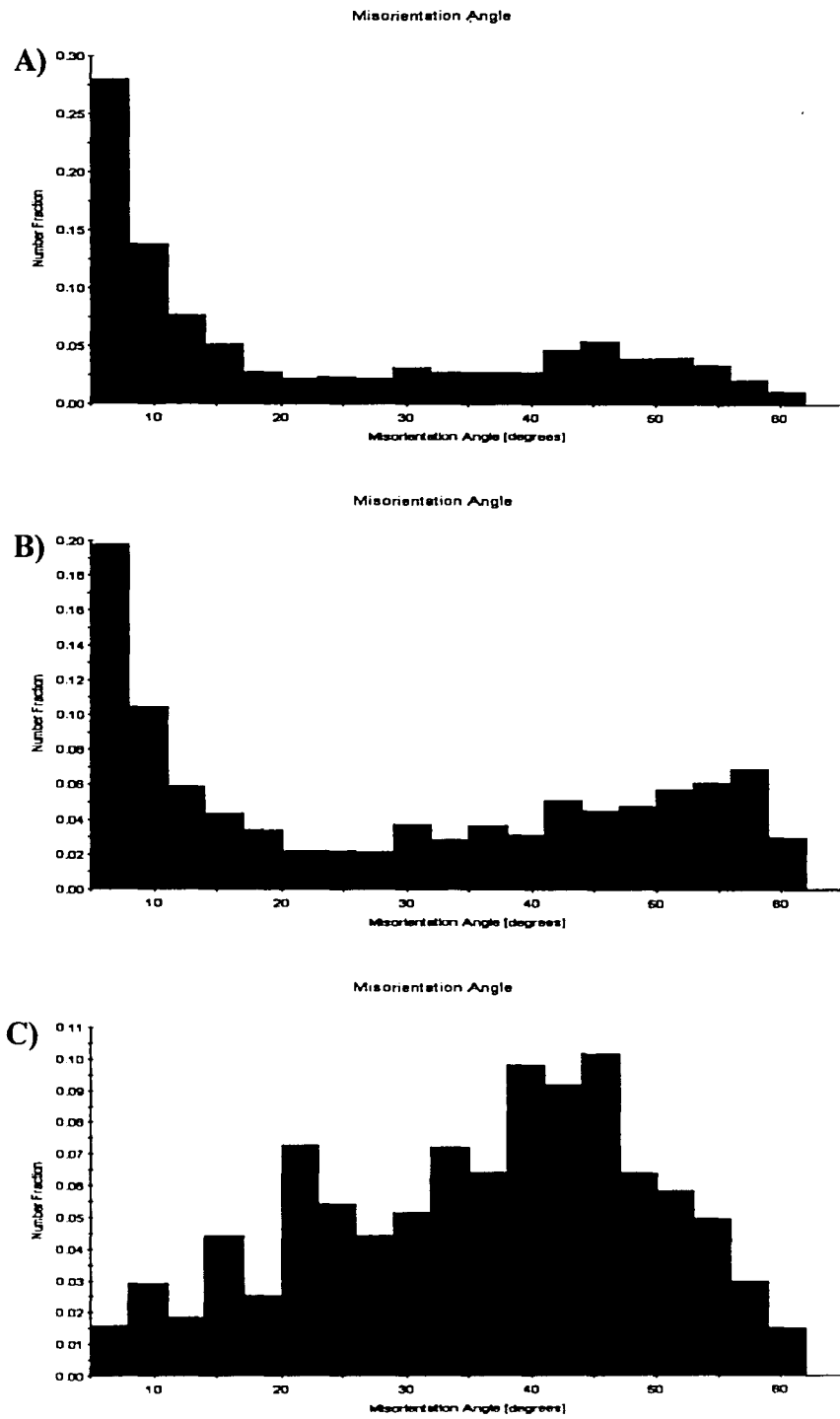


**Figure 33.** Misorientation histograms for EBSD scans taken at the surface of a sample with high Cr content deformed to a 75% reduction in a single pass at 400°C (750°F) (Condition H). A) 3 second anneal, B) 5 second anneal, C) 7 second anneal

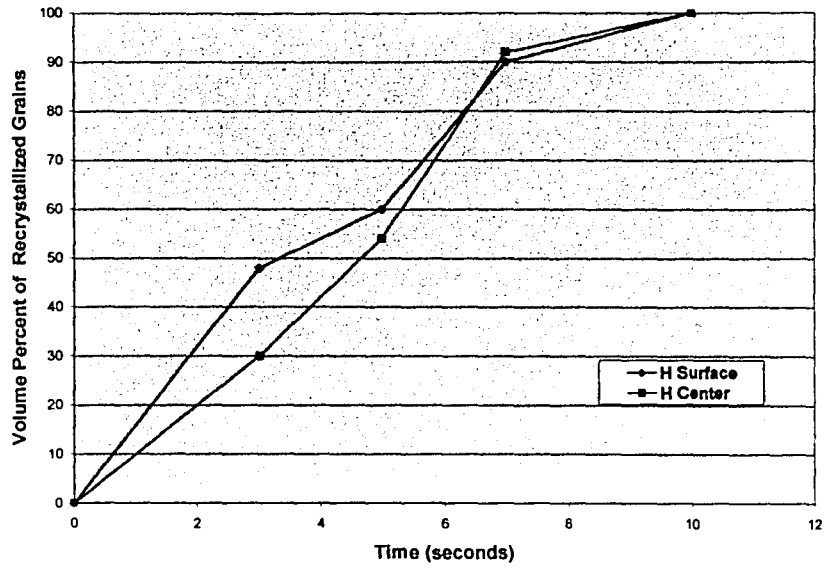


**Figure 34.** Percent of recrystallized grains for processing condition H at the surface and center

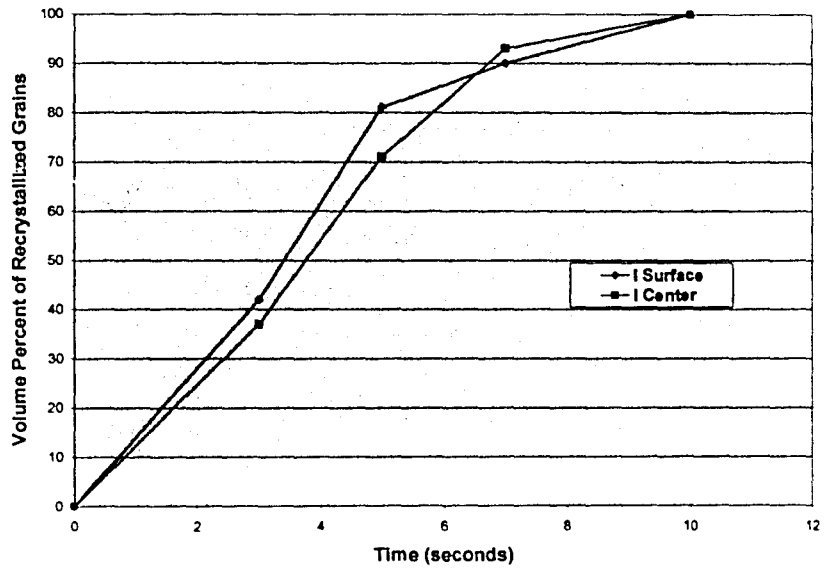


**Figure 35.** Percent of recrystallized for processing condition I at the surface and center

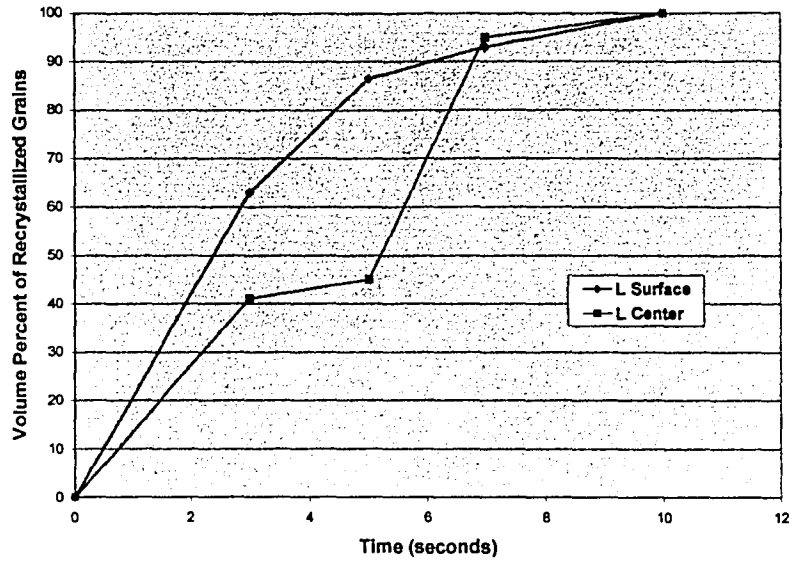


**Figure 36.** Percent of recrystallized grains for processing condition L at the surface and center

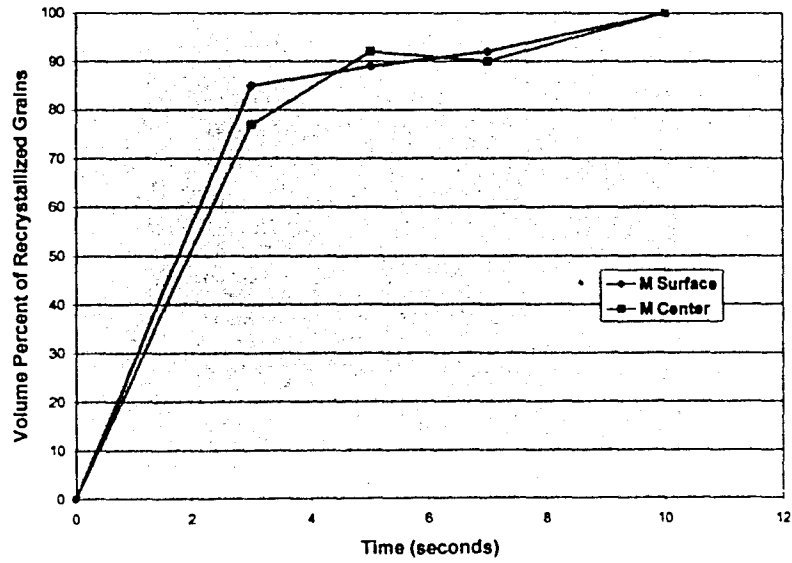


**Figure 37.** Percent of recrystallized for processing condition M at the surface and center

## 4.0 Discussion and Future Work

### 4.1 Discussion of Recrystallization Kinetics

Deformation processing has a large effect on the microstructure and the mechanical properties of a deformed sheet. In the case of hot rolling, variables such as rolling temperature, strain, single pass or multi pass rolling schedule, deformation zone geometry, which is a function of the rolled pass thickness reduction and working roll geometry, and alloy chemistry will have an impact on the stored energy and kinetics of recrystallization. Isolating each of these parameters allows for a comparison of the recrystallization kinetics. It is important to isolate each of the parameters because hot rolling of aluminum is a complex process with various competing mechanisms of recrystallization. In general, material that was processed at high strains, low temperature, and a low Cr:Mn ratios showed the most elevated kinetics of recrystallization. It is also important to note that for Figures 23 – 28 and Figures 34 – 37 there are no error bars present because of limited sample availability.

The effect of alloy chemistry in AA6061 is clearly shown in Figures 23 and 24. These two graphs plot the volume percent of recrystallized grains in the LOM images versus annealing time for two processing conditions with high and low Cr content. From these figures it can be concluded that the material that possessed the higher Cr:Mn ratio exhibited slower recrystallization kinetics. This is to be expected for these conditions because Cr will act to suppress recovery and

boundary motion during annealing which will slow down the growth rate of recrystallized grains.

The total deformation measured by reduction in thickness also had a significant affect on the stored energy and subsequent kinetics of recrystallization during annealing. Figures 25 and 26 show the difference in percent of recrystallized grains versus time for samples deformed to 75% and 90% reductions. The samples that experienced higher levels of total strain during deformation showed elevated kinetics due to higher levels of stored energy. The higher levels of stored energy contribute to a higher driving force for static recrystallization during annealing which increases kinetics. Also when comparing the 90% reduction versus the 75% reduction, the 90% reduction will create a smaller average grain size because of the higher levels of strain associated with the larger total deformation. The smaller average grain size will provide a higher number of high angle boundaries that will have the driving force to grow and consume surrounding deformed material. Because of the increased potential for nucleation and the higher stored energy associated with higher strain levels, the kinetics of recrystallization for a more highly deformed material should be elevated versus a lesser deformed sample.

Temperature was also observed to have an affect on the kinetics of recrystallization during annealing. Figure 27 shows a comparison of two sets of samples processed under the same conditions at two different deformation temperatures of 482°C (900°F) and 400°C (750°F). The results from this graph

follow the accepted trends for recrystallization when considering temperature variation. Material that was rolled at the lower temperature showed higher kinetics versus the material that was deformed at the higher temperature. The difference in kinetics can once again be attributed to the stored energy in the sample after deformation. For deformation that occurs at lower temperatures, a larger amount of stored energy will be created versus a sample deformed at a higher temperature. This increase in stored energy for hot rolled aluminum sheet can be explained by an increase in flow stress associated with deformation at lower temperatures and recovery mechanisms. As the flow stress increases, the material is more resistant to deformation and, therefore, the dislocation density will increase which adds more stored energy. This increase in stored energy supplies a larger driving force for recrystallization which will elevate the kinetics of recrystallization. An increased deformation temperature will also increase the potential for any dynamic recovery mechanisms in hot rolled AA6061 sheet. Because aluminum is a high stacking fault material, dislocation climb and cross-slip occur readily during hot deformation which can aid in removing some of the dislocation density accumulated during deformation [11]. This process of dynamic recovery will help lower the stored energy of the system in two ways. The first will be by general annihilation of dislocations during the hot rolling process that will lower the overall stored energy of the system. Secondly, the recovery process will help in lowering the flow stress of the work piece during deformation by minimizing dislocation tangle. This will have an overall affect on lowering the stored energy

and will ultimately lower the kinetics of recrystallization of a sample rolled at an elevated temperature.

Finally, Figure 28 shows the effects of a single pass deformation versus a multi-pass rolling schedule on the volume percent of recrystallized grains versus annealing time for the same overall reduction of 90%. This figure shows no distinct difference in the kinetics of recrystallization of a single pass deformation versus the multi-pass schedule. Both processes appear to follow similar trends, with the single pass material showing a steeper change in the volume percent of recrystallized grains present between the annealing times of 5 and 7 seconds while the multi-pass sample shows a more smooth transition. Because the multi-pass samples were annealed for thirty minutes between each pass, a majority of the stored energy created during deformation was removed because of the inter-pass anneal. This means for the multi-pass schedule shown in Figure 28, although the total reduction is 90%, the stored energy created during deformation more closely resembles a 66.7% reduction as shown in Table V for the final pass of the multi-pass deformation. Because of this difference in deformation, the 90% single pass reduction exhibited a more dramatic change in recrystallization kinetics versus the 90% multi-pass deformation because of the interpass anneal that helped remove a large portion of the prior deformation.

## 4.2 Recrystallization Kinetics

Results from the PLOM analysis showed a variation in recrystallization kinetics from the surface to the center of the hot rolled samples upon annealing. To further investigate this phenomena EBSD areas scans were used. Only four of the thirteen total processing conditions were chosen for the EBSD analysis because not all of the conditions upon annealing showed partially recrystallized material. Four sets of conditions were chosen that possessed a partially recrystallized state so the kinetics could be determined. Overall, the results from these scans showed a difference in kinetics at the surface of the sample versus the mid-thickness.

When comparing Figures 29 and 30, there are distinct differences in the microstructure that can be seen. Both figures represent the microstructure after a five second anneal with Figure 29 representing the surface and Figure 30 representing the center of the annealed sample. The surface appears to be completely recrystallized after five seconds while the center image shows areas of deformed microstructure. This shows that there is a gradient present in the microstructure from the surface to the center that can be related back to the stored energy created during deformation.

One of the major factors contributing to this deviation from uniform strain during deformation is the temperature gradient created during processing [24]. During hot rolling of aluminum alloys this temperature gradient can come from several sources. The first and most significant source in creating a thermal



gradient is related to the difference in temperature between the work piece and the rolls. For the hot rolled samples in this experiment there were thermal differences of 300°C (570°F) and 382°C (720°F) between the work piece and the working rolls for the two deformation temperatures. This creates a flux of heat out of the sample during deformation that creates a thermal gradient within the sample which contributes to a gradient in stored energy. Upon annealing the effect of this gradient is seen in the difference of recrystallization kinetics at the surface of the sample versus the center (Figure 19D). It is also important to note that there are other sources of heat flux into the sample during deformation as well. Friction between the rolls and work piece add heat to the system during deformation along with the reduction in thickness. Overall the thermal gradient that exists during hot rolling is created by several competing factors, but the results from this work show that the kinetics of recrystallization at the surface of the deformed sheet are elevated when compared to the center.

The second factor contributing to difference in recrystallization kinetics between the center and the surface of the deformed sample is related to the strain gradient present during deformation (Figures 29 and 30). This gradient arises from several factors. First, friction exists between the surface of the rolls and work piece. This friction allows for the surface and the mid-thickness of the sample to travel at different velocities creating a shear stress which will contribute to the gradient in stored energy. Also, the deformation zone geometry aids in determining the gradient in stored energy. Because the material is deformed to

such high strains there will be a strong presence of redundant deformation that will aid in creating a stored energy gradient from the surface to the center of the deformed sheet.

The EBSD analysis also showed the presence of fine equiaxed grains at the surface of the annealed samples (Figure 32). This microstructure showed a strong resemblance to cDRX or gDRX grains that are formed from serrated high angle boundaries during deformation to high strains. The presence of fine, equiaxed grains have been seen in extrusion for this alloy and have also been attributed to different types of dynamic recrystallization phenomena [26 - 28]. The literature has also shown for this alloy, deformed in torsion to large strains ( $\epsilon_{\text{eff.}} > 2.5$ ) and similar deformation temperatures to this set of experiments, that this fine-equiaxed structure will develop at the sample surface [27]. Upon annealing, the sample surface will exhibit faster kinetics of recrystallization when compared to the center of the material because of the increased availability of nucleation sites associated with the fine equiaxed grains when compared to the larger more elongated grains present in the center (Figure 30). These results suggest that along with the temperature and strain gradients created during hot rolling, there is also a microstructural evolution component created during hot rolling that aids in creating a non-uniform microstructure during annealing. When predicting the overall kinetics of recrystallization, it is clear that understanding the role of the starting microstructure is critical

### 4.3 Quantitative Analysis of Recrystallization Kinetics

A quantitative analysis was performed on all of the EBSD area scans to determine the volume percent of recrystallized grains present at each of the annealing times for the surface and mid-thickness of each sample. This analysis was performed using misorientation histograms and summing all misorientations between  $5^{\circ}$  –  $15^{\circ}$  degrees and treating that sum as the fraction of deformed grains present in the sample. This number is then subtracted from 100% and will give the volume fraction of recrystallized grains present at a given annealing time and processing condition. Figures 34 – 37 show the graphical representation of the volume percent of recrystallized grains versus time for the center and mid-thickness for each of the samples. These plots follow the expected trend with the surface showing elevated kinetics versus the center, but the difference presented by Figures 34 - 37 are not significant. An explanation for this small difference in the kinetics of recrystallization between the surface and center of the samples can be related to the processing conditions for each of the samples used for the EBSD area scans. Because these samples experienced the most severe levels of strain at lower temperatures, the microstructural gradient is not large due to a relatively uniform strain distribution. Therefore, the kinetics at the surface and the center will be highly elevated based on stored energy. This means that a sample would often show a similar level of recrystallized structure at the center and the surface

because the kinetics were fast enough to not allow for the development of partially recrystallized state through the thickness of the sample. The elevated kinetics can be seen in Figure 37. When comparing the misorientation histograms to the EBSD area scan associated with it, the calculated values do not always correspond precisely. Often times images that appear to have a completely recrystallized structure by visual inspection, will only have calculated values of 90% recrystallized using the misorientation histogram calculations. The reason for this discrepancy is suspected to be related to the surface preparation technique. Despite chemical polishing, there are still areas on the surface and subsurface of the sample that have higher dislocation densities because of surface deformation experienced during preparation. Because the EBSD analysis is very sensitive, it is able to identify this deformation however it is not related to the hot rolling deformation. This phenomenon will cause the calculations for volume percent of recrystallized grains to be lower than expected.

#### **4.4 Future Work**

The research conducted on hot rolling of AA6061 was completed to better understand the kinetics of recrystallization during annealing. The physical metallurgy data that was generated during these experiments could be used as input data for Finite Element Modeling (FEM) purposes. A comparison of the modeling work along with the physical metallurgy could aid in developing a

software package that could more accurately predict the microstructural evolution during hot rolling.

Further work needs to be completed to understand how the multi-pass schedule affects the microstructural evolution during hot rolling and annealing. It is important to understand the cumulative affects of multiple passes, along with inter-pass heat treatments, on the resulting microstructure and texture. Examining the microstructure between deformation steps will help gain a better understanding of the industrial hot rolling process.

A more in depth investigation into the effects of texture components on recrystallization could help in understand the very complex recrystallization phenomena during hot rolling. Finally, to complete these texture analyses, an improvement on the sample preparation technique will be needed. To get more precise recrystallization data and finer detail about the material texture, a surface preparation technique will have to be developed that minimizes any surface deformation created during deformation.

## 5.0 Conclusions

This research has investigated the kinetics of recrystallization for hot rolled AA6061 that was flash annealed for various times. From this work, the following conclusions can be made:

- Hot rolled AA6061 follows traditional static recrystallization kinetics behavior when considering total strain, rolling temperature, rolling schedule, and Cr content even at short annealing times. Material that possessed the high Cr:Mn ratio exhibited retarded recrystallization kinetics during flash annealing. Also, samples processed at higher temperatures and lower total strains exhibited slower kinetics of recrystallization which can be attributed to lower levels of stored energy created during deformation.
- Due to the high levels of deformation that some of the samples experienced during processing and subsequent heat treatment, the kinetics of recrystallization were elevated. Evidence from this research shows that some samples showed a completely recrystallized structure within two seconds at 912°F (490°C).
- Based on limited sample availability the observed kinetics of recrystallization for the flash annealing experiments for all of the processing conditions followed the general trend proposed by the JMAK curve.

- EBSD area scans proved to be a useful tool in determining the fraction of recrystallized present at various annealing times. To improve on the precision of this technique an improved surface preparation procedure must be established to minimize any surface deformation that is created during mechanical grinding and polishing.
- A microstructural gradient was present in the hot rolled aluminum alloys after flash annealing. This non-uniform microstructure can be attributed to strain and temperature gradients created during hot rolling. Through the use of EBSD area scans at the sample surface and mid-thickness, a quantitative analysis was performed to show the difference in kinetics between these two areas of the deformed material. This strain gradient was created by friction between the rolls and the sample surface, and temperature gradients that exist in the material during hot rolling.
- EBSD analysis showed the presence of a fine equiaxed microstructure at the surface of the deformed sample. This microstructure, which resembled a cDRX or gDRX microstructure, also played an important role in elevating the kinetics of recrystallization at the surface of the sample versus the center during annealing.

## 7.0 References

1. I.J. Polmear. Light Metals: Metallurgy of Light Metals, Halsted Press, 1995.
2. The Aluminum Association, Aluminum Standards and Data, 1993.
3. Matsuda, Kenji; Ikeno, Susumu; Matsui, Hiroaki; Sato, Tatsuo; Terayama, Kiyoshi; Uetani, Yasuhiro. *Comparison of Precipitates between Excess Si-Type and Balanced-Type Al-Mg-Si Alloys during Continuous Heating*. Metallurgical and Materials Transactions A, Volume 36, Number 8, August 2005, pp. 2007- 2012(6).
4. Jack W. Bray. *Aluminum Mill and Engineered Wrought Prod: Physical Met*, ASM Handbook Online Ed.
5. Olaf Engler, Jurgen Hirsch. *Texture Control by Thermomechanical Processing of AA6xxx Al-Mg-Si sheet alloys for Automotive Applications – A Review*. Materials Science and Engineering A336 (2002) 249 – 262.
6. George E. Dieter. Workability Testing Techniques. American Society for Materials, 1984.
7. George E. Dieter. Mechanical Metallurgy, McGraw – Hill, 1986.
8. William F. Hosford, Robert M. Caddell, Metal Forming: Mechanics and Metallurgy, Prentice – Hall, 1983.
9. P. M. Cook, *Proc Conf. Properties of Materials at High Rates of Strain*, Institution of Mechanical Engineers, London, 1957, pp. 85-97.
10. R.D. Doherty, *Panel Discussion on Rx Textures*, ICO-TOM 8, TMS, Warrendale, PA, 1988, p. 369.
11. J.J. Jonas, C.M. Sellars, W.J. Tegart. (1969), *Metallurgical Reviews*, 130, 1.
12. C. Chovet, S. Gourdet, F. Montheillet, *Large Strain Deformation Textures and Microstructures of an Al-Mg-Si Alloy*, Materials Science Forum, vol. 331 – 337, 2000, p. 733.



13. R.D. Doherty, D.A. Hughes, F.J. Humphreys, J.J. Jonas, D. Juul Jensen, M.E. Kassner, W.E. King, T.R. McNelley, H.J. McQueen, A.D. Rollet, *Current Issues in Recrystallization: a review*, Materials Science and Engineering A238 (1997) 219 – 274.
14. W.A. Anderson, R.F. Mehl. (1945), Trans. Metall. Soc. A.I.M.E. 161, p140.
15. F.J Humphreys, M. Hatherly, Rx and Related Annealing Phenomena, Pergamon, 1995.
16. R.A. Vandermeer, B.B. Rath (1989a), Metall. Trans. A, 20A, 391.
17. B.L Adams, S.I. Wright, K. Kunze, Metall Trans, 24A (1993), 819-831.
18. M. Hatherly (1982), Proc. 6<sup>th</sup> Int. Conf. on Strength of Metals and Alloys, ed. Gifkins, Pergamon, Oxford 1181.
19. J.C. Blade, P.L. Morris (1975), Proc. 4<sup>th</sup> Int. Conference on Textures. Cambridge, 171.
20. Y. Zou, K.W. Neale, Int. J. Mech. Sci. 37 (1995) 1.
21. P.S. Bate, Scripta Metall. Mater. 27 (1992) 515.
22. U.F. Kocks, C.N. Tome, H.-R. Wenk, Texture and Anisotropy, Cambridge University Press, 1998, p. 171-177.
23. F.J. Humphreys, *Review Grain and subgrain characterization by electron back scatter diffraction*, Journal of Materials Science 36 (2001) 3833 – 3854.
24. D. Dingley. *Progressive steps in the development of electron back scatter diffraction and orientation imaging microscopy*, Journal of Microscopy, Vol. 213 Pt 3 March 2004, pp. 214 – 224.
25. M. Y. Huh, K. R. Lee, O. Engler, *Evolution of texture and strain states in AA 3004 sheet during rolling with a dead block*, International Journal of Plasticity, Vol. 20, Issue7, July 2004, pp. 1183 – 1197.
26. William H. Van Geertruyden, Heather M. Browne, Wojciech Z. Misiolek, Paul T. Wang, Metallurgical and Materials Transactions A, Volume 36, Number 4, April 2005, pp. 1049-1056(8)

28. William H. Van Geertruyden, "The Origin of Surface Recrystallization in Extrusion of 6xxx Aluminum Alloys", PhD Dissertation, Lehigh University April, 2004.
29. H. Browne, "Evolution of Dead Metal Zone During Indirect Extrusion of 6061 Aluminum Alloys", MS Thesis, Lehigh University, April 2004.

## VITA

Neil was born to David and Janet Hurley on September 21, 1981 in Tiffin, Ohio. After graduating from Council Rock High School in Newtown PA in 2000, Neil began attending Lehigh University with an interest in engineering. In 2004, Neil graduated cum laude from Lehigh University with a Bachelor's of Science degree in Materials Science and Engineering. He was awarded the Allen S. Quier Prize during his senior year for outstanding academic achievement in scholastic work by the faculty of the Materials Science and Engineering department at Lehigh University. Neil has also co-authored a conference paper on aluminum hot rolling microstructural evolution and he has given a technical presentation at Alcoa Technical Center in Monroeville, Pa on aluminum hot rolling characterization. Upon graduation, Neil will be pursuing employment in industry.

**END OF  
TITLE**